Relativistic Distance Based and Bond Additive Topological Descriptors of Zeolite RHO Materials

Micheal Arockiaraj[a], **Daniel Paul**[b], **Sandi Klavžar**[c,d,e], **Joseph Clement**[f,*], **Sushil Tigga**[a], **Krishnan Balasubramanian**[g]

[a]Department of Mathematics, Loyola College, Chennai 600034, India

[b]Department of Mathematics, Sri Sairam Institute of Technology, Chennai 600044, India

[c]Faculty of Mathematics and Physics, University of Ljubljana, Slovenia

[d]Faculty of Natural Sciences and Mathematics, University of Maribor, Slovenia

[e]Institute of Mathematics, Physics and Mechanics, Ljubljana, Slovenia

[f]Department of Mathematics, School of Advanced Sciences, Vellore Institute of Technology, Vellore 632014, India

[g]School of Molecular Sciences, Arizona State University, Tempe AZ 85287-1604, USA

Abstract

Topological indices are graph invariants which provide quantitative information on molecular structures and thus they yield quantitative structure activity relationships (QSAR) and quantitative structure property relationships (QSPR) for the prediction of physico chemical properties of compounds. The zeolite RHO frameworks have received considerable attention as they are extremely useful in trapping heavy metal ions and thus in environmental remediation. These frameworks contain optimal cavities to trap toxic medial ions and recently for heavier halogen substitution. We have applied an efficient technique to obtain exact analytical expressions for the various relativistic topological descriptors of the zeolite RHO structures by graph-theoretical cut methods that reduce the complex structures with tunnels and cages into simpler graphs. Our incorporation of relativistic parameters would be especially useful for the characterization of properties when heavier atoms are incorporated.

Keywords: Graph metrics; topological indices; cut method; zeolites; relativistic QSAR of materials.

*Corresponding author : clementjmail@gmail.com

1 Introduction

Zeolites are crystalline microporous aluminosilicates with uniform cavities that can trap multiple toxic metal ions and environmental pollutant gases. Zeolite RHO is a material with considerable potential as it offers smaller pore sizes of $3.6\mathring{A} \times 3.6\mathring{A}$ with a relatively low Si/Al ratio of $2.5 - 3.0$. The zeolite offers significant flexibility during sorptions and thus these materials offer considerable promise to trap multiple metal ions of varying sizes such as Na^+, Cd^{2+}, Sr^{2+}, Rb^+, Ba^{2+} etc. Moreover they have also been considered as potential candidates for the environmental remediation of high level nuclear wastes. The structure of zeolite RHO consists of a body centered cubic arrangement of α-cages linked via double 8-rings [1] as shown in Figure 1. This framework displays a considerable flexibility during the sorption-desorption process with metal ions and molecules, and thus it is able to adapt to various cation sizes and shaped adsorbent molecules [2, 3]. Johnson et al. [4] have reported the synthesis of a microporous aluminogermanate with a zeolite RHO topology of composition $Na_{16}Cs_8Al_{24}Ge_{24}O_{96}$. In this framework cation (sodium and cesium) sites can be substituted by a number of cations such as NH_4^+, Ba^{2+}, Sr^{2+} and Cd^{2+} etc. [4], thus acting as sorption sites for such metal ions. More recently Sun et al. [5] have reported a novel high-silica zeolite RHO that included a self-assembled Cs^+-18-crown -6 sandwich complex. The crown complex containing Cs^+ exhibits a greater catalytic activity for ethanol dehydration than other materials with a considerably enhanced selectivity toward ethylene. Zeolite RHO exhibits a high selectivity in catalyzing the production of dimethylamine from ammonia and methanol [6–11]. In addition, it can also serve as a hydrogen storage material with tailor-made pore sizes and cations that are suitable for hydrogen absorption [12–14] or as a CO_2 selective adsorbent [15]. The aluminosilicate framework of zeolite RHO undergoes a significant distortion and loss of symmetry upon dehydration. Ng et al. [16] have used an ultraviolet irradiation method for faster and efficient synthesis of zeolite RHO; the technique has yielded high crystallinity with a truncated octahedral morphology. Hence molecular sieves and zeolites are becoming important materials for gas sorptions catalysis and environmental remediation through sorption of toxic heavy metal ions including high level radioactive wastes [17,18] as they offer flexible pore size to accommodate multiple ions. Furthermore, heavier halogen substitution such as Br in scapolite-group minerals and sodalite has received experimental and mineralogical interest [19]. Typically the solid samples of these materials are characterized with X-ray diffraction (XRD), field emission scanning electron microscopy (FESEM), Fourier transform infrared spectroscopy (FTIR), thermogravimetric analysis (TGA) and nitrogen adsorption-desorption analysis in order to establish their structures and pore sizes.

The design of new materials as well as proposed materials with novel architecture require theoretical insights and knowledge concerning feasible structures, their topologies, as well as short and long-

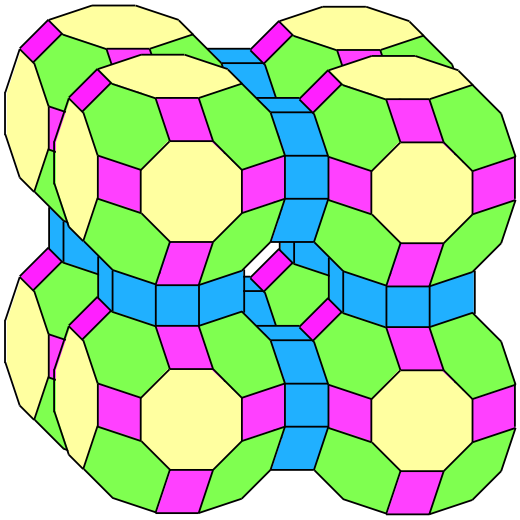

Figure 1: Zeolite RHO structure

range orders. The topology of the zeolite RHO material is directly connected to tiling and sphere packings [20]. The nomenclature of each material is based on its zeolite framework type and it is assigned a three letter code usually derived from the name of the source material; the code is used in describing the network of corner sharing tetrahedral of the atoms irrespective of its composition [21–23].

Chemical graph theory is a branch of discrete mathematics which facilitates the computation of topological descriptors of molecular structures which can then be used to predict the physico chemical properties of complex systems such as zeolite RHO materials. Molecular graphs are structural representations, where the vertices represent the atoms in the molecular structure and the edges represent the chemical bonds. As properties of molecules are functions of their structures, real numbers derived from the associated molecular graphs are called the graph invariants or more frequently structural descriptors (topological indices). In the study of QSAR and QSPR these parameters are utilized to compute the physico chemical and biological activities of chemical compounds from their molecular structures. In this regard, a topological index can be regarded as a score function which maps each molecular structure to a real number and then used as a descriptor of the molecule under consideration.

In the present study we consider the computation of relativistic topological indices for zeolite RHO materials that can incorporate heavy ions such as Cs^{+}, Ba^{2+}, Sr^{2+}, Cd^{2+} , Hg^{2+}, Br^{-} as well as heavy metal oxide ions like ${UO_2}^{2+}$ that are present in high level nuclear wastes. For such systems containing very heavy atoms, relativistic effects including spin-orbit coupling alter the geometries, energetics, topological and reactivity properties of these compounds are extremely important [24–27]. Thus any realistic development of topological indices must include the relativistic parameters into both vertices and edges of the molecular structures. Consequently, the present study considers such a development of topological indices that incorporate relativistic effects. Furthermore we have validated the derived

analytical results for the topological indices of zeolite RHO networks by computing several of the topological indices by the software Topochemie-2020 [67].

2 Computational Techniques

We start with some basic definitions and notations that will be used in the paper. Let G be a finite simple connected graph with vertex set and edge set respectively as $V(G)$ and $E(G)$. We define $d_G(u,v)$ to be the usual shortest-path distance between vertices $u, v \in V(G)$ and the distance between a vertex $u \in V(G)$ and an edge $f = xy \in E(G)$ is defined as $d_G(u,f) = \min\{d_G(u,x), d_G(u,y)\}$. Moreover, the shortest-path distance between edges $g = ab$ and $f = xy$ is defined as $D_G(g,f) = \min\{d_G(a,f), d_G(b,f)\}$. For an edge $e = uv \in E(G)$, we propose the values $n_u(e|G)$ and $m_u(e|G)$ are defined as the number of vertices and edges of G respectively whose distance to the vertex u is smaller than the distance to the vertex v. Similarly, $n_v(e|G)$ and $m_v(e|G)$ are defined as the number of vertices and edges of G respectively whose distance to the vertex v is smaller than the distance to the vertex u.

Let $\deg_G(u)$ be the number of edges that incident to u and the degree of an edge $e = uv \in E(G)$ is defined as the number of edges adjacent to e and denoted by $\deg_G(e)$. i.e., $\deg_G(e) = \deg_G(u) + \deg_G(v) - 2$. In addition to the degree measure of the edge, there are two types of measures defined based on the degrees of end vertices and given below:

- $w^+(e) = \deg_G(u) + \deg_G(v)$.
- $w^*(e) = \deg_G(u)\deg_G(v)$.

We now present the definitions of Wiener-type, Szeged-type, Mostar-type and degree-based topological indices for a simple graph G [28–50].

(1) Wiener-type indices:

Wiener	$W(G)$	$= \sum_{\{u,v\}\subseteq V(G)} d_G(u,v)$
Edge Wiener	$W_e(G)$	$= \sum_{\{f,g\}\subseteq E(G)} D_G(f,g)$
Vertex-edge Wiener	$W_{ev}(G)$	$= \frac{1}{2}\sum_{u\in V(G)}\sum_{f\in E(G)} d_G(u,f)$
Schultz	$S(G)$	$= \sum_{\{u,v\}\subseteq V(G)} (\deg_G(u) + \deg_G(v)) d_G(u,v)$

Gutman $Gut(G) = \sum_{\{u,v\}\subseteq V(G)} \deg_G(u)\deg_G(v)d_G(u,v)$

(2) Szeged-type indices:

Vertex Szeged $Sz_v(G) = \sum_{e=uv\in E(G)} n_u(e|G)n_v(e|G)$

Edge Szeged $Sz_e(G) = \sum_{e=uv\in E(G)} m_u(e|G)m_v(e|G)$

Edge-vertex Szeged $Sz_{ev}(G) = \frac{1}{2}\sum_{e=uv\in E(G)} (n_u(e|G)m_v(e|G) + n_v(e|G)m_u(e|G))$

Padmakar-Ivan $PI(G) = \sum_{e=uv\in E(G)} (m_u(e|G) + m_v(e|G))$

w^+-vertex Szeged $w^+Sz_v(G) = \sum_{e=uv\in E(G)} w^+(e)\ n_u(e|G)n_v(e|G)$

w^+-edge Szeged $w^+Sz_e(G) = \sum_{e=uv\in E(G)} w^+(e)\ m_u(e|G)m_v(e|G)$

w^+-Padmakar-Ivan $w^+PI(G) = \sum_{e=uv\in E(G)} w^+(e)\ (m_u(e|G) + m_v(e|G))$

w^*-vertex Szeged $w^*Sz_v(G) = \sum_{e=uv\in E(G)} w^*(e)\ n_u(e|G)n_v(e|G)$

w^*-edge Szeged $w^*Sz_e(G) = \sum_{e=uv\in E(G)} w^*(e)\ m_u(e|G)m_v(e|G)$

w^*-Padmakar-Ivan $w^*PI(G) = \sum_{e=uv\in E(G)} w^*(e)\ (m_u(e|G) + m_v(e|G))$

(3) Mostar-type indices:

Mostar $Mo(G) = \sum_{e=uv\in E(G)} \left|n_u(e|G) - n_v(e|G)\right|$

Edge Mostar $Mo_e(G) = \sum_{e=uv\in E(G)} \left|m_u(e|G) - m_v(e|G)\right|$

w^+-Mostar $w^+Mo(G) = \sum_{e=uv\in E(G)} w^+(e)\ \left|n_u(e|G) - n_v(e|G)\right|$

w^+-edge Mostar $w^+Mo_e(G) = \sum_{e=uv\in E(G)} w^+(e)\ \left|m_u(e|G) - m_v(e|G)\right|$

w^*-Mostar $w^*Mo(G) = \sum_{e=uv\in E(G)} w^*(e)\ \left|n_u(e|G) - n_v(e|G)\right|$

w^*-edge Mostar	$w^*Mo_e(G) = \sum_{e=uv\in E(G)} w^*(e)\ \big\lvert m_u(e\vert G) - m_v(e\vert G)\big\rvert$

(4) Degree-based indices:

First Zagreb	$M_1(G) = \sum_{e=uv\in E(G)} w^+(e)$
Second Zagreb	$M_2(G) = \sum_{e=uv\in E(G)} w^*(e)$
Randić	$R(G) = \sum_{e=uv\in E(G)} \frac{1}{\sqrt{w^*(e)}}$
Atom Bond Connectivity	$ABC(G) = \sum_{e=uv\in E(G)} \sqrt{\frac{w^+(e)-2}{w^*(e)}}$
Harmonic	$H(G) = \sum_{e=uv\in E(G)} \frac{2}{w^+(e)}$
Sum Connectivity	$SC(G) = \sum_{e=uv\in E(G)} \frac{1}{\sqrt{w^+(e)}}$
Hyper Zagreb	$HM(G) = \sum_{uv\in E(G)} (w^+(e))^2$
Geometric Arithmetic	$GA(G) = \sum_{e=uv\in E(G)} 2\frac{\sqrt{w^*(e)}}{w^+(e)}$
Irregularity Measure	$irr(G) = \sum_{e=uv\in E(G)} \big\lvert \deg_G(u) - \deg_G(v)\big\rvert$
Sigma	$\sigma(G) = \sum_{e=uv\in E(G)} \big(\deg_G(u) - \deg_G(v)\big)^2$
Forgotten	$F(G) = \sum_{e=uv\in E(G)} \big(\deg_G(u)^2 + \deg_G(v)^2\big)$
Symmetric Division Degree	$SDD(G) = \sum_{e=uv\in E(G)} \left(\frac{\deg_G(u)}{\deg_G(v)} + \frac{\deg_G(v)}{\deg_G(u)}\right)$

We expand this preliminary section by defining a few concepts related to the cut method [52, 53], which has been used in the computation of relativistic topological descriptors of certain types of zeolite structures [23, 51]. A subgraph H of a graph G is said to be isometric if $d_H(u,v) = d_G(u,v)$ holds for all pairs of vertices u and v of H. The family of graphs that comprises of all isometric subgraphs of hypercubes are known as partial cubes. The Djoković-Winkler relation Θ [54, 55], which acts a decisive part in our computations, is defined as follows: if $e = ab \in E(G)$ and $f = cd \in E(G)$, then $e\Theta f$ if $d_G(a,c) + d_G(b,d) \neq d_G(a,d) + d_G(b,c)$. The relation Θ is reflexive and symmetric, but not

transitive in general. If G is a partial cube, then Θ is also transitive and hence G is an equivalence relation. Moreover, in that case for any Θ-class F_i, the graph $G - F_i$ consists of exactly two connected components [52]. We now define the measures of F_i based on w^+ and w^* as $w^+(F_i) = \sum_{s \in F_i} w^+(s)$, and $w^*(F_i) = \sum_{s \in F_i} w^*(s)$. The standard cut method for the computation of topological indices [48,50,55–64] can be now expressed as follows.

Theorem 2.1. *Let G be a partial cube with its Θ-partition $\mathcal{F} = \{F_1, \ldots, F_k\}$. For each $1 \leq i \leq k$, let XF_i and YF_i be the connected components of G. Let $n_1(F_i) = |V(XF_i)|$, $n_2(F_i) = |V(YF_i)|$, $m_1(F_i) = |E(XF_i)|$ and $m_2(F_i) = |E(YF_i)|$. Then*

1. $W(G) = \sum_{i=1}^{k} n_1(F_i)\ n_2(F_i)$,
2. $W_e(G) = \sum_{i=1}^{k} m_1(F_i)\ m_2(F_i)$,
3. $W_{ev}(G) = \sum_{i=1}^{k} \frac{1}{2}[n_1(F_i)\ m_2(F_i) + n_2(F_i)\ m_1(F_i)]$,
4. $Sz_v(G) = \sum_{i=1}^{k} |F_i|\ n_1(F_i)\ n_2(F_i)$,
5. $Sz_e(G) = \sum_{i=1}^{k} |F_i|\ m_1(F_i)\ m_2(F_i)$,
6. $Sz_{ev}(G) = \sum_{i=1}^{k} \frac{1}{2}\ |F_i|\ \{n_1(F_i)\ m_2(F_i) + n_2(F_i)\ m_1(F_i)\}$,
7. $PI(G) = |E(G)|^2 - \sum_{i=1}^{k} |F_i|^2$,
8. $S(G) = |E(G)||V(G)| + \sum_{i=1}^{k} 2[n_1(F_i)\ m_2(F_i) + n_2(F_i)\ m_1(F_i)]$,
9. $Gut(G) = 2|E(G)|^2 + \sum_{i=1}^{k} [4m_1(F_i)\ m_2(F_i) - |F_i|^2]$,
10. $Mo(G) = \sum_{i=1}^{k} |F_i|\ \big|n_1(F_i) - n_2(F_i)\big|$,
11. $Mo_e(G) = \sum_{i=1}^{k} |F_i|\ \big|m_1(F_i) - m_2(F_i)\big|$,

    When $\# \in \{+, *\}$,

12. $w^{\#}Mo(G) = \sum_{i=1}^{k} w^{\#}(F_i)\ \big|n_1(F_i) - n_2(F_i)\big|$,
13. $w^{\#}Mo_e(G) = \sum_{i=1}^{k} w^{\#}(F_i)\ \big|m_1(F_i) - m_2(F_i)\big|$,

14. $w^{\#}Sz_v(G) = \sum_{i=1}^{k} w^{\#}(F_i)\ n_1(F_i)\ \ n_2(F_i)$,

15. $w^{\#}Sz_e(G) = \sum_{i=1}^{k} w^{\#}(F_i)\ m_1(F_i)\ m_2(F_i)$,

16. $w^{\#}PI(G) = \sum_{i=1}^{k} w^{\#}(F_i)\ (m_1(F_i) + m_2(F_i))$.

3 A Construction of Partial Cubes

In order to apply Theorem 2.1, we need to deal with partial cubes. To establish this fact for the key players of this paper, zeolite RHO materials, the theorem proved in this section is essential. To prove it, we recall the following two result, see [65, Lemma 11.2] and [65, Lemma 11.3], respectively.

Lemma 3.1. *Let G be a bipartite graph and $e = uv$, $f = xy$ be two edges of G with $e\Theta f$. Then the notation can be chosen such that $d_G(u,x) = d_G(v,y) = d_G(u,y) - 1 = d_G(v,x) - 1$.*

Lemma 3.2. *Suppose that a walk P connects the endpoints of an edge e but does not contain it. Then P contains an edge f with $e\Theta f$. If it is the only edge of P with this property, then it cannot be incident with e.*

To state the key result recall that a subgraph H of a graph G is convex if for each pair of vertices x and y of G, each shortest path between x and y in G lies completely in H, and that a set of edges of G is called a perfect matching if it an independent edge set that covers every vertex of G.

Theorem 3.1. *Let G and H be partial cubes, and let C_G and C_H be convex cycles in G and H, respectively, where $|C_G| = |C_H|$. Let X be the graph obtained from the disjoint union of G and H by adding a perfect matching between C_G and C_H which induces an isomorphism between C_G and C_H. Then X is a partial cube.*

Proof. To prove the result we will use Winkler's characterization that a connected graph G is a partial cube if and only if G is bipartite and Θ is transitive on $E(G)$ [55]. First, since G and H are partial cubes, they are bipartite graphs. It is then straightforward to see that X is bipartite as well. It remains to show that Θ is transitive in X.

Let $e_1 = x_1y_1$, $e_2 = x_2y_2$, and $e_3 = x_3y_3$ be arbitrary edged of X such that $e_1\Theta e_2$ and $e_2\Theta e_3$ hold. We need to prove that $e_1\Theta e_3$ holds as well. If $e_1, e_2, e_3 \in E(G)$, then since G is convex in X and G is a partial cube, $e_1\Theta e_3$ holds by Wikler's theorem applied to G (as a subgraph of X). Similarly, if $e_1, e_2, e_3 \in E(H)$, we have the same conclusion.

Consider next the case that e_1 is one of the matching edges between G and H. Assume without loss of generality that $x_1 \in V(G)$ and $y_1 \in V(H)$. Then $d_X(y_1, u) = d_X(x_1, u) + 1$ holds for each

vertex $u \in V(G)$. Using Lemma 3.1 it follows that e_1 is not in relation Θ with any of the edges from $E(G)$. So e_1 can be only in relation Θ with matching edges. It is straighforward to see that e_1 is indeed in relation Θ with all the matching edges. In particular, e_2 and e_3 are also matching edges and $e_1 \Theta e_3$ holds.

It remains to consider the case in which two of the edges e_1, e_2, e_3 lie in $E(G)$ and one in $E(H)$ or the other way around. Without loss of generality, there are two cases to be considered: (i) $e_1, e_2 \in E(G)$ and $e_3 \in E(H)$, and (ii) $e_1, e_3 \in E(G)$ and $e_2 \in E(H)$.

Suppose first that $e_1, e_2 \in E(G)$ and $e_3 \in E(H)$. Recall that $e_1 \Theta e_2$ and $e_2 \Theta e_3$. By Lemma 3.1 we may assume that $d_X(x_2, x_3) = d_X(y_2, y_3) = d_X(x_2, y_3) - 1 = d_X(y_2, x_3) - 1$. Let P be an arbitrary shortest x_2, x_3-path and let u be the first vertex on P which lies in C_G. Denoting the neighbor of u in H by u' we may assume that u' also lies on P. Since $d_X(y_2, x_3) = d_X(x_2, x_3) + 1$, we infer that $d_X(y_2, u) = d_X(x_2, u) + 1$. Consider next a shortest y_2, y_3-path Q, and let w be the first vertex of Q that lies on C_G. Then $w \neq u$, for otherwise we would have $d_X(y_3, u') < d_X(x_3, u')$ which is not possible because it would imply that $d_X(y_3, x_2) < d_X(x_3, x_2)$. Consider now the walk W which connects x_2 with y_2 and is composed of the subpath of P between x_2 and u, a shortest path between u and w on C_G, and the subpath of Q between w and y_2. By Lemma 3.2, W contains an edge f such that $e_2 \Theta f$. Since no two edges of a shortest path are in relation Θ, we infer that f must be an edge of the cycle C_G. Because $e_1 \Theta e_2$, $e_2 \Theta f$, and $e_1, e_2, f \in E(G)$, we get that $e_1 \Theta f$. Denoting by f' the isomorphic copy of f in C_H we also get that $e_1 \Theta f'$. But then, since the distance function between the end vertices of e_1 and f', and between f' and e_3 is additive, we conclude that $e_1 \Theta e_3$.

Suppose second that $e_1, e_3 \in E(G)$ and $e_2 \in E(H)$, where again $e_1 \Theta e_2$ and $e_2 \Theta e_3$. Considering the edges e_1 and e_2 and using an argument parallel to the above reasoning, we find that there exists an edge $f \in C_G$ such that $e_1 \Theta f$. Let f' be the isomorphic copy of f in C_H. Similarly, considering the edges e_3 and e_2 we find that there exists an edge $g \in C_G$ such that $e_3 \Theta g$. Let g' be the isomorphic copy of g in C_H. Since $f' \Theta e_2$ and $e_2 \Theta g'$, and H is a partial cube, we see that $f' \Theta g'$. Consequently, $f \Theta g$. But now we have $e_1 \Theta f \Theta g \Theta e_3$, and as these are all edges of G (which is a partial cube and a convex subgraph of X), transitivity implies that $e_1 \Theta e_3$. □

4 Results and Discussion

The primitive unit cell of zeolite RHO materials is a truncated cuboctahedron, called the α-cage. It is an Archimedean solid consisting of 48 vertices and 72 edges with 26 faces made of 12 squares, 8 hexagons and 6 octagons that preserve the point group symmetry on each its face as depicted in Figure 2(a). That this α-cage, that is, the truncated cuboctahedron, belongs to the class of partial cubes has

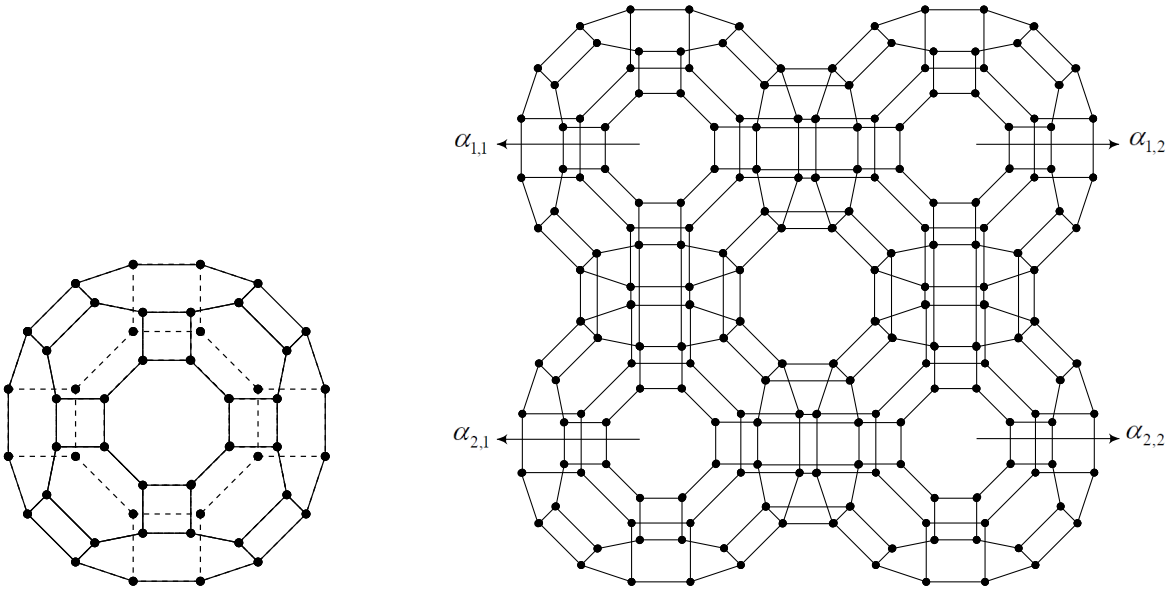

(a) α–cage (b) $RHO(2,2)$

Figure 2: Primitive unit cell of zeolite RHO and its single layer

been shown in [66] where an extensive search for cubic partial cubes has been performed.

The zeolite RHO materials are designed by arranging the α-cages in a 3D mesh $a \times b \times c$ such that two α-cages are connected by two eight-membered rings (octagonal prism) in order that all cation sites are equally accessible for adsorbate molecules as shown in Figure 2(b). This 3D materials is denoted by $RHO(a,b,c)$ and by symmetrical arrangement of α-cages, $RHO(a,b,c) \cong RHO(b,c,a) \cong RHO(c,a,b)$. Inductively applying Theorem 3.1, we infer that the 3D material $RHO(a,b,c)$ is a partial cube.

From the octagonal-prism arrangement of α-cages, we can find the number of vertices and edges as $|V(RHO(a,b,c))| = 48abc$ and $|E(RHO(a,b,c))| = 96abc - 8\,(ab+bc+ca)$, respectively. It is clear that $RHO(a,b,c)$ contains abc number of α-cages and we denote the α-cage in the (x,y,z) position of $a \times b \times c$ mesh as $\alpha_{x,y,z}$.

The relativistic parameters for the various heavy atoms impregnated into zeolites can be derived by convenient localization of molecular orbitals as described in [51]. Hence, the topological indices in terms of relativistic quantum parameters can be computed by weighted graphs with weights γ_{x} and ρ_{xy} for each vertex x and edge xy, respectively. Thus, the molecular graphs of doped or impregnated zeolite RHOs with heavy elements can be represented as a structural graphs with vertex-weights $\{\gamma_{\mathrm{x}}, \gamma_{\mathrm{y}}\}$ and edge-weights ρ_{xy} such that γ_{x} and γ_{y} with equal ratio. Let $V_\gamma(RHO(a,b,c))$ and $E_\rho(RHO(a,b,c))$ be the structural vertex set and edge set of $RHO(a,b,c)$ respectively. Therefore, it can be seen that $|V_\gamma(RHO(a,b,c))| = \frac{1}{2}\{\gamma_{\mathrm{x}} + \gamma_{\mathrm{y}}\}|V(RHO(a,b,c))|$ and $|E_\rho(RHO(a,b,c))| = \rho_{\mathrm{xy}}|E(RHO(a,b,c))|$.

We now present the technique to compute the relativistic topological indices for single layered zeolite RHO materials, i.e. $RHO(a, b, 1)$ and then readily generalize the technique to multi-layered layers zeolite $RHO(a, b, c)$. For convenience, we use the notation $RHO(a, b)$ instead of $RHO(a, b, 1)$ and in the same way $\alpha_{x,y,1}$ by $\alpha_{x,y}$ as given in Figure 2(b). To proceed further, we first compute the Θ-classes of single α-cage and then identify the Θ-classes of $RHO(a, b)$.

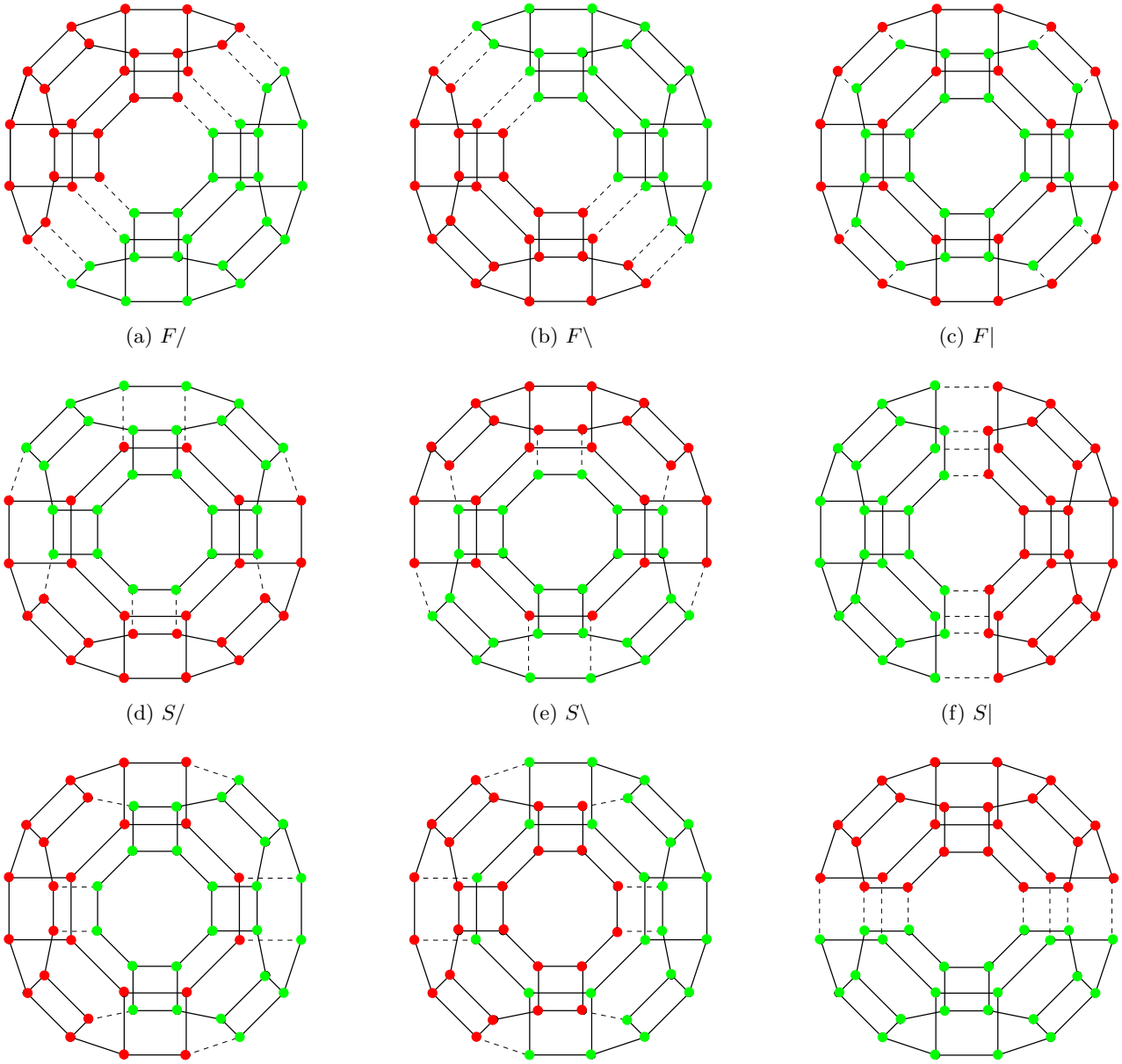

(a) $F/$ (b) $F\backslash$ (c) $F|$

(d) $S/$ (e) $S\backslash$ (f) $S|$

(g) $T/$ (h) $T\backslash$ (i) $T|$

Figure 3: Various Θ-classes of α-cage based on the front-, side- and top-view

As a consequence of point group symmetry on each face of α-cage, we could find nine types of Θ-classes as shown in Figure 3. These types are denoted by front-view forward-slash $F/$, front-view

backward-slash $F\backslash$, front-view vertical-slash $F|$, side-view forward-slash $S/$, side-view backward-slash $S\backslash$, side-view vertical-slash $S|$, top-view forward-slash $T/$, top-view backward-slash $T\backslash$, and top-view vertical-slash $T|$.

Theorem 4.1. *Let G be a zeolite RHO materials $RHO(a,b)$ where $1 \leq a \leq b$. Then,*

(1) $W(G) = \frac{48}{5}a(\gamma_{\rm x}+\gamma_{\rm y})^2(60ab^3+(40a^2+15a+5)b^2+(10a^3+5a)b-2a^4+2)$.

(2) $W_e(G) = \frac{16}{15}\rho_{\rm xy}^2((7260a^2-1320a+60)b^3+(4840a^3-5100a^2+1565a-45)b^2+(1210a^4-1320a^3+1595a^2-90a-15)b-242a^5+50a^3-45a^2+237a)$.

(3) $W_{ev}(G) = \frac{32}{5}a\rho_{\rm xy}(\gamma_{\rm x}+\gamma_{\rm y})((330a-30)b^3+(220a^2-75a+35)b^2+(55a^3-30a^2+35a)b-11a^4+11)$.

(4) $Sz_v(G) = 384a\rho_{\rm xy}(\gamma_{\rm x}+\gamma_{\rm y})^2((23a^2+1)b^3+3a^2b-a^3+a)$.

(5) $Sz_e(G) = \frac{256}{15}\rho_{\rm xy}^3((6800a^3-2130a^2+790a-30)b^3+(-2570a^3+315a^2-85a)b^2+(165a^4+1430a^3-360a^2+25a)b-11a^5-320a^4+25a^3+320a^2-44a)$.

(6) $Sz_{ev}(G) = \frac{128}{5}a\rho_{\rm xy}^2(\gamma_{\rm x}+\gamma_{\rm y})((1250a^2-195a+85)b^3+(-235a^2-5)b^2+(15a^3+195a^2-30a)b-a^4-55a^3+5a^2+55a-4)$.

(7) $PI(G) = \frac{128}{3}\rho_{\rm xy}^2((180a^2-39a+3)b^2+(-42a^2+3a)b+a^3+3a^2-a)$.

(8) $S(G) = \frac{64}{5}a\rho_{\rm xy}(\gamma_{\rm x}+\gamma_{\rm y})((660a-60)b^3+(440a^2+15a+55)b^2+(110a^3-60a^2+55a)b-22a^4+22)$.

(9) $Gut(G) = \frac{64}{15}\rho_{\rm xy}^2((7260a^2-1320a+60)b^3+(4840a^3-1485a^2+845a)b^2+(1210a^4-1320a^3+845a^2-30a-15)b-242a^5+60a^3+227a)$.

(10) $Mo(G) = 96\rho_{\rm xy}(\gamma_{\rm x}+\gamma_{\rm y})((10a^2-2a+(-1)^a-1)b^2-2a^2b-((-1)^{a+b}+(-1)^b-2)a^2)$.

(11) $Mo_e(G) = \frac{32}{3}\rho_{\rm xy}^2((330a^2-84a+33(-1)^a-33)b^2+(-78a^2+12a-3(-1)^a+3)b-2a^3-(33(-1)^{a+b}-33(-1)^b-66)a^2+(3(-1)^{a+b}-3(-1)^b+8)a)$.

(12) $w^+Mo(G) = 16\rho_{\rm xy}(\gamma_{\rm x}+\gamma_{\rm y})((456a^2-144a+45(-1)^a-21)b^2+(-150a^2-9(-1)^a+9)b+2a^3-(42(-1)^{a+b}-45(-1)^b+51)a^2+(3(-1)^{a+b}-9(-1)^b+10)a)$.

(13) $w^+Moe(G) = 16\rho_{\rm xy}^2((1672a^2-618a+165(-1)^a-69)b^2+(-612a^2+84a-48(-1)^a+40)b-2a^3+(-154(-1)^{a+b}+165(-1)^b-179)a^2+(25(-1)^{a+b}-48(-1)^b+59)a+2(-1)^{a+b}-5)$.

(14) $w^*Mo(G) = 8\rho_{\rm xy}^2(\gamma_{\rm x}+\gamma_{\rm y})((1752a^2-750a+171(-1)^a+21)b^2+(-798a^2+24a-63(-1)^a+63)b+16a^3+(-150(-1)^{a+b}+171(-1)^b-57)a^2+(24(-1)^{a+b}-63(-1)^b+71)a)$.

(15) $w^*Moe(G) = \frac{8}{3}\rho_{xy}^3((19272a^2-9276a+1881(-1)^a+405)b^2+(-9504a^2+1512a-864(-1)^a+648)b+76a^3+(-1650(-1)^{a+b}+1881(-1)^b-453)a^2+(414(-1)^{a+b}-864(-1)^b+842)a+39(-1)^{a+b}-102)$.

(16) $w^+Szv(G) = \frac{384}{5}\rho_{xy}(\gamma_x+\gamma_y)^2((880a^3-55a^2-25a+30)b^3+(-45a^3-15a)b^2+(-5a^4+45a^3-15a^2)b+a^5-35a^4+30a^3+35a^2-a)$.

(17) $w^+Sze(G) = \frac{128}{15}\rho_{xy}^3((103960a^3-39100a^2+7185a+2975)b^3+(-44050a^3+10020a^2-2330a-660)b^2+(1705a^4+16145a^3-6195a^2+780a+25)b-33a^5-4480a^4+3750a^3+3820a^2-717a)$.

(18) $w^+PI(G) = \frac{64}{3}\rho_{xy}^2((2748a^2-837a+75)b^2+(-879a^2+144a-3)b+14a^3+75a^2-17a)$.

(19) $w^*Szv(G) = \frac{192}{5}\rho_{xy}^2(\gamma_x+\gamma_y)^2((3400a^3-395a^2-355a+240)b^3+(-315a^3-105a)b^2+(-40a^4-105a^3-105a^2)b+8a^5-125a^4+240a^3+125a^2-8a)$.

(20) $w^*Sze(G) = \frac{64}{15}\rho_{xy}^4((401320a^3-172670a^2+6655a+25765)b^3+(-184990a^3+55680a^2-11090a-5280)b^2+(3410a^4+38655a^3-24960a^2+4030a+215)b+418a^5-16000a^4+28555a^3+10720a^2-2993a)$.

(21) $w^*PI(G) = \frac{64}{3}\rho_{xy}^3((5298a^2-2043a+198)b^2+(-2118a^2+459a-12)b+25a^3+198a^2-37a)$.

Proof. We begin the proof by identifying the Θ-classes of $RHO(a,b)$ based on the Θ-classes of α-cage as shown in Figure 4. For $1 \le i \le a+b-1$, let $F/_i = \{e \in \alpha_{x,y} : e \text{ is in } F/ \text{ such that } x+y-1=i\}$, $F\backslash_i = \{e \in \alpha_{x,y} : e \text{ is in } F\backslash \text{ such that } y-x+a=i\}$ and $F|_1 = \{e \in \alpha_{x,y} : e \text{ is in } F|\}$ be the front-view type of Θ-classes. For $1 \le i \le a$, let $S/_i = \{e \in \alpha_{x,y} : e \text{ is in } S/ \text{ such that } x=i\}$, $S\backslash_i = \{e \in \alpha_{x,y} : e \text{ is in } S\backslash \text{ such that } x=i\}$ and $1 \le i \le b$, $S|_i = \{e \in \alpha_{x,y} : e \text{ is in } S| \text{ such that } y=i\}$ be the side-view type of Θ-classes. For $1 \le i \le b$, let $T/_i = \{e \in \alpha_{x,y} : e \text{ is in } T/ \text{ such that } y=i\}$, $T\backslash_i = \{e \in \alpha_{x,y} : e \text{ is in } T\backslash \text{ such that } y=i\}$ and $1 \le i \le a$, $T|_i = \{e \in \alpha_{x,y} : e \text{ is in } T| \text{ such that } x=i\}$ be the top-view type of Θ-classes.

For $1 \le i \le b-1$, let $S\text{–}_i$ be a set of edges connecting $\alpha_{x,i}$ and $\alpha_{x,i+1}$, called side-view horizontal-slash type Θ-classes. Similary, for $1 \le i \le a-1$, let $T\text{–}_i$ be a set of edges connecting $\alpha_{i,y}$ and $\alpha_{i+1,y}$, called top-view horizontal-slash type Θ-classes. Since $|V(RHO(a,b))| = 48ab$ and $|E(RHO(a,b))| = 8[11ab-(a+b)]$, we have $|V_\gamma(RHO(a,b))| = \frac{1}{2}\{\gamma_x+\gamma_y\}|V(RHO(a,b))|$ and $|E_\rho(RHO(a,b))| = \rho_{xy}|E(RHO(a,b))|$. The graph theoretical parameters of Front-view Θ-classes are given below:

$$|F/_i| = \begin{cases} 8i\rho_{xy} & \text{if } 1 \le i \le a-1 \\ 8a\rho_{xy} & \text{if } a \le i \le b \\ \left|F/_{a+b-i}\right| & \text{if } b+1 \le i \le a+b-1 \end{cases}$$

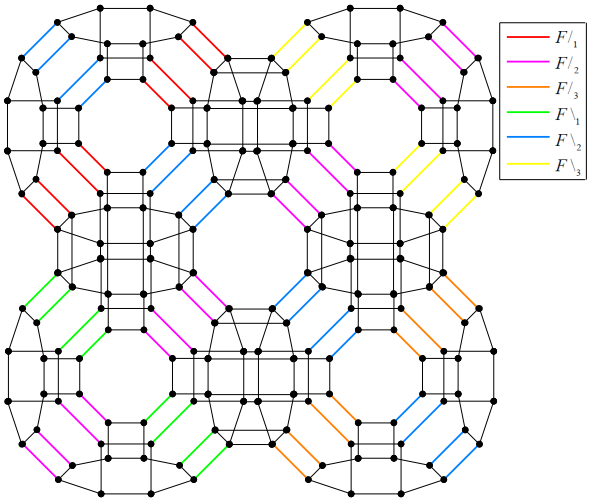

(a) $F/_1, F/_2, F/_3$ & $F\backslash_1, F\backslash_2, F\backslash_3$ in RHO(2,2)

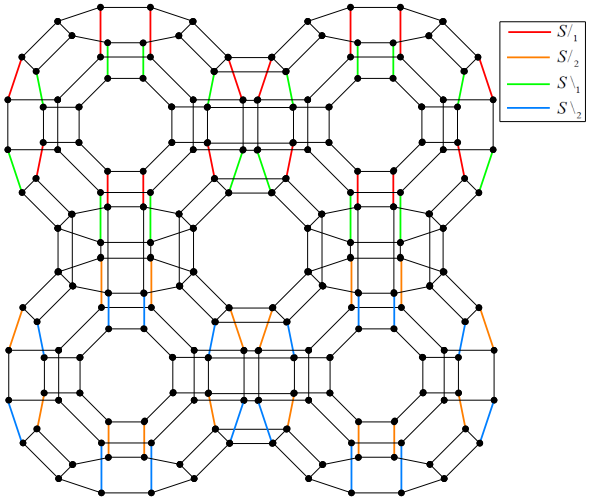

(b) $S/_1, S/_2$ & $S\backslash_1, S\backslash_2$ in RHO(2,2)

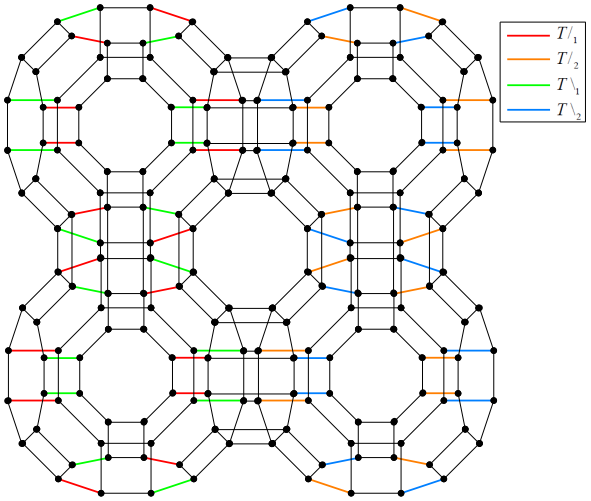

(c) $T/_1, T/_2$ & $T\backslash_1, T\backslash_2$ in RHO(2,2)

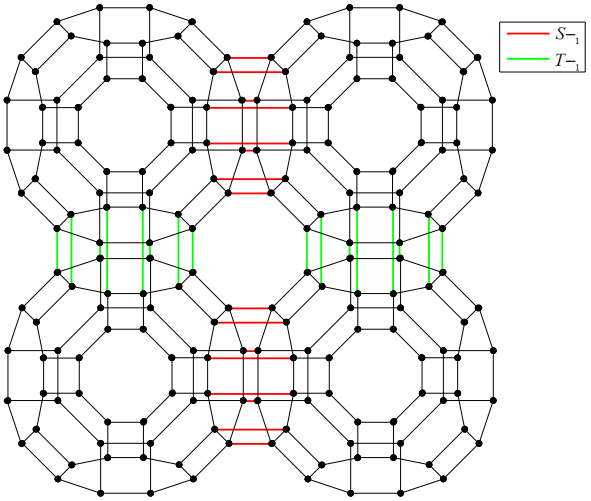

(d) $S-_1$ & $T-_1$ in RHO(2,2)

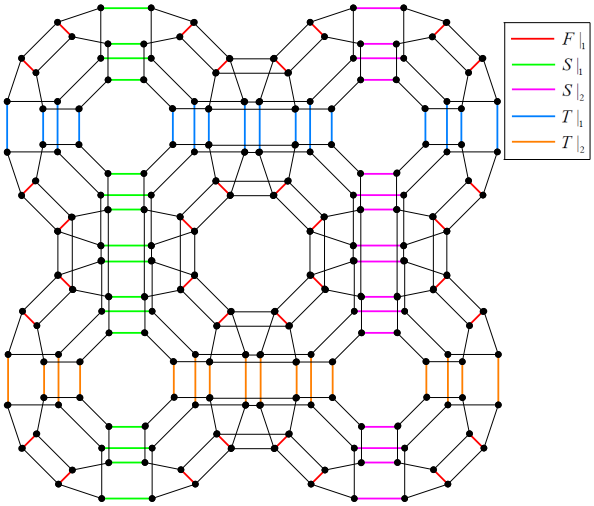

(e) $F|_1$, $S|_1$, $S|_2, T|_1$ & $T|_2$ in RHO(2,2)

Figure 4: Various Θ-classes of $RHO(2,2)$ based on the front-, side-, top-, horizontal- and vertical-view

$$n_1(F/_i) = \begin{cases} 12i^2\{\gamma_{\mathrm{x}} + \gamma_{\mathrm{y}}\} & \text{if } 1 \leq i \leq a-1 \\ 12a(2i-a)\{\gamma_{\mathrm{x}} + \gamma_{\mathrm{y}}\} & \text{if } a \leq i \leq b \\ n_1(F/_{a+b-i}) & \text{if } b+1 \leq i \leq a+b-1 \end{cases}$$

$$n_2(F/_i) = |V_\gamma(RHO(a,b))| - n_1(F/_i),$$

$$m_1(F/_i) = \begin{cases} 4i(11i-3)\rho_{\mathrm{xy}} & \text{if } 1 \leq i \leq a-1 \\ \{8(11a-1)i - 4a(11a+1)\}\rho_{\mathrm{xy}} & \text{if } a \leq i \leq b \\ m_1(F/_{a+b-i}) & \text{if } b+1 \leq i \leq a+b-1 \end{cases}$$

$$m_2(F/_i) = |E_\rho(RHO(a,b))| - m_1(F/_i) - |F/_i|\,.$$

$$w^+(F/_i) = \begin{cases} 4(14i-1)\rho_{\mathrm{xy}} & \text{if } 1 \leq i \leq a-1 \\ 8(7a-1)\rho_{\mathrm{xy}} & \text{if } i = a,\ a = b \\ 2(28a-3)\rho_{\mathrm{xy}} & \text{if } i = a,\ a < b \\ 4(14a-1)\rho_{\mathrm{xy}} & \text{if } a < i < b \\ w^+\left(F/_{a+b-i}\right) & \text{if } b \leq i \leq a+b-1 \end{cases}$$

$$w^*(F/_i) = \begin{cases} 4(25i-4)\rho_{\mathrm{xy}}^2 & \text{if } 1 \leq i \leq a-1 \\ 4(25a-7)\rho_{\mathrm{xy}}^2 & \text{if } i = a,\ a = b \\ 2(50a-11)\rho_{\mathrm{xy}}^2 & \text{if } i = a,\ a < b \\ 4(25a-4)\rho_{\mathrm{xy}}^2 & \text{if } a < i < b \\ w^*\left(F/_{a+b-i}\right) & \text{if } b \leq i \leq a+b-1 \end{cases}$$

$$|F|_1| = 8ab\rho_{\mathrm{xy}},$$

$$n_1(F|_1) = n_2(F|_1) = 12ab\{\gamma_{\mathrm{x}} + \gamma_{\mathrm{y}}\},$$

$$m_1(F|_1) = m_2(F|_1) = (40ab - 4(a+b))\rho_{\mathrm{xy}},$$

$$w^+(F|_1) = 8(8ab - (a+b))\rho_{\mathrm{xy}},$$

$$w^*(F|_1) = 4(32ab - 7(a+b))\rho_{\mathrm{xy}}^2.$$

The graph theoretical parameters of $S/$ and $S\backslash$ as well as $T/$ and $T\backslash$ are the same. In addition, the parameters of $S/$ and $T/$ are symmetrical with respect to a and b whereas $S|$ and $T|$ as well as

$S-$ and $T-$ are symmetrical with respect to b and a. Hence, we have the following measures for only S-type classes.

$$
\begin{aligned}
|S/_i| &= 8b\rho_{\mathrm{xy}}, \quad 1 \le i \le a \\
n_1\left(S/_i\right) &= 12b(2i-1)\{\gamma_{\mathrm{x}}+\gamma_{\mathrm{y}}\}, \quad 1 \le i \le a \\
n_2\left(S/_i\right) &= |V_\gamma(RHO(a,b))| - n_1\left(S/_i\right), \quad 1 \le i \le a \\
m_1\left(S/_i\right) &= \{8(11b-1)i - 4(13b-1)\}\rho_{\mathrm{xy}}, \quad 1 \le i \le a \\
m_2\left(S/_i\right) &= |E_\rho(RHO(a,b))| - m_1\left(S/_i\right) - |S/_i|, \quad 1 \le i \le a
\end{aligned}
$$

$$
w^+\left(S/_i\right) = \begin{cases} 4(15b-2)\rho_{\mathrm{xy}} & \text{if } i = 1, a \\ 8(8b-1)\rho_{\mathrm{xy}} & \text{if } 1 < i < a \end{cases}
$$

$$
w^*\left(S/_i\right) = \begin{cases} 28(4b-1)\rho_{\mathrm{xy}}^2 & \text{if } i = 1, a \\ 4(32b-7)\rho_{\mathrm{xy}}^2 & \text{if } 1 < i < a \end{cases}
$$

$$
\begin{aligned}
|S|_i| &= 8a\rho_{\mathrm{xy}}, \quad 1 \le i \le b \\
n_1\left(S|_i\right) &= 12a(2i-1)\{\gamma_{\mathrm{x}}+\gamma_{\mathrm{y}}\}, \quad 1 \le i \le b \\
n_2\left(S|_i\right) &= |V_\gamma(RHO(a,b))| - n_1\left(S|_i\right), \quad 1 \le i \le b \\
m_1\left(S|_i\right) &= \{8(11a-1)i - 4(13a-1)\}\rho_{\mathrm{xy}}, \quad 1 \le i \le b \\
m_2\left(S|_i\right) &= |E_\rho(RHO(a,b))(\rho_{\mathrm{xy}})| - m_1\left(S|_i\right) - |S/_i|, \quad 1 \le i \le b \\
w^+\left(S|_i\right) &= 8(7a-1)\rho_{\mathrm{xy}}, \quad 1 \le i \le b \\
w^*\left(S|_i\right) &= 4(25a-7)\rho_{\mathrm{xy}}^2, \quad 1 \le i \le b
\end{aligned}
$$

$$
\begin{aligned}
|S-_i| &= 8a\rho_{\mathrm{xy}}, \quad 1 \le i \le b-1 \\
n_1\left(S-_i\right) &= 24ai\{\gamma_{\mathrm{x}}+\gamma_{\mathrm{y}}\}, \quad 1 \le i \le b-1 \\
n_2\left(S-_i\right) &= |V_\gamma(RHO(a,b))| - n_1\left(S-_i\right), \quad 1 \le i \le b-1 \\
m_1\left(S-_i\right) &= \{8(11a-1)i - 8a\}\rho_{\mathrm{xy}}, \quad 1 \le i \le b-1 \\
m_2\left(S-_i\right) &= |E_\rho(RHO(a,b))| - m_1\left(S-_i\right) - |S/_i|, \quad 1 \le i \le b-1 \\
w^+\left(S-_i\right) &= 64a\rho_{\mathrm{xy}}, \quad 1 \le i \le b-1 \\
w^*\left(S-_i\right) &= 128a\rho_{\mathrm{xy}}^2, \quad 1 \le i \le b-1
\end{aligned}
$$

If we denote $TI(X)$ to represent the numerical number induced by the class X with respect to TI, then the proof is complete by the following equation.

$$TI(G) = 4\ \sum_{i=1}^{a-1} TI(F/_i) +\ 2\ \sum_{i=a}^{b} TI(F/_i) + TI(F|_1)$$
$$+\ 2\ \sum_{i=1}^{a} TI(S\backslash_i) + \sum_{i=1}^{b} TI(S|_i) + \sum_{i=1}^{b-1} TI(S-_i)$$
$$+\ 2\ \sum_{i=1}^{b} TI(T\backslash_i) + \sum_{i=1}^{a} TI(T|_i) + \sum_{i=1}^{a-1} TI(T-_i).$$

□

Theorem 4.2. *Let* $TI \in \{W, W_e, W_{ev}, Sz_v, Sz_e, Sz_{ev}, PI, S, Gut, Mo, Mo_e, w^+Mo, w^+Mo_e, w^*Mo, w^*Mo_e, w^+Sz_v, w^+Sz_e, w^+PI, w^*Sz_v, w^*Sz_e, w^*PI\}$. *For* $a \leq b \leq c$,

$$TI(RHO(a,b,c)) = TI(a,b,c) + TI(a,c,b) + TI(b,c,a),$$

where we use $TI(a,b,c)$ *from the following expressions,* $TI(a,c,b)$ *and* $TI(b,c,a)$ *are obtained from* $TI(a,b,c)$ *by replacing suitable values.*

(1) $W(a,b,c) = \frac{48}{5}ac(\gamma_{\mathrm{x}} + \gamma_{\mathrm{y}})^2((20ab^2)c^2 + (-2a^4 + 10a^3b + 20ab^3 + 2)c - 5ab^2)$.

(2) $W_e(a,b,c) = \frac{16}{15}\rho_{\mathrm{xy}}^2(2880a^2b^2 - 480a^2b + 20a^2 - 480ab^2 + 40ab + 20b^2)c^3 + (288a^5 + 1440a^4b - 480a^3b + 10a^3 + 2880a^2b^3 - 2880a^2b^2 + 270a^2b - 480ab^3 + 240ab^2 + 240ab + 278a + 20b^3 - 20b)c^2 + (48a^5 - 240a^4b + 40a^3b - 480a^2b^3 + 240a^2b^2 + 60a^2b - 5a^2 + 40ab^3 + 60ab^2 - 30ab - 48a - 5b^2)c - 2a^5 + 10a^4b + 20a^2b^3 - 60a^2b^2 + 2a)$.

(3) $W_{ev}(a,b,c) = \frac{16}{5}ac\rho_{\mathrm{xy}}(\gamma_{\mathrm{x}} + \gamma_{\mathrm{y}})((20ab - 240ab^2 + 20b^2)c^2 + (24a^4 - 120a^3b + 20a^2b - 240ab^3 + 120ab^2 + 20b^3 - 10b - 24)c - 2a^4 + 10a^3b + 20ab^3 + 30ab^2 - 5ab - 5b^2 + 2)$.

(4) $Sz_v(a,b,c) = 384a^2c\rho_{\mathrm{xy}}(\gamma_{\mathrm{x}} + \gamma_{\mathrm{y}})^2((-a^2 + 8ab^3 + 2ab + 1)c^2 - ab^3)$.

(5) $Sz_e(a,b,c) = \frac{128}{15}a\rho_{\mathrm{xy}}^3((-24a^4 + 360a^3b - 755a^3 + 5760a^2b^3 - 1920a^2b^2 + 1550a^2b + 120a^2 - 960ab^3 + 160ab^2 - 600ab + 755a + 40b^3 + 40b - 96)c^3 + (2a^4 - 30a^3b + 120a^3 - 1920a^2b^3 + 240a^2b^2 - 240a^2b - 10a^2 + 160ab^3 + 50ab - 120a + 8)c^2 + (-5a^3 + 140a^2b^3 + 60a^2b^2 + 5a^2b + 60ab^3 - 10ab^2 + 5a - 5b^3)c - 60a^2b^3)$.

(6) $Sz_{ev}(a,b,c) = \frac{128}{5}ac\rho_{\mathrm{xy}}^2(\gamma_{\mathrm{x}} + \gamma_{\mathrm{y}})((-a^4 + 15a^3b - 60a^3 + 480a^2b^3 - 80a^2b^2 + 120a^2b + 5a^2 - 40ab^3 - 25ab + 60a - 4)c^2 + (5a^3 - 80a^2b^3 - 10a^2b - 5a)c - 30a^2b^3 + 5a^2b^2 + 5ab^3)$.

(7) $PI(a,b,c) = \frac{64}{3}\rho_{\mathrm{xy}}^2((2a^3 + 144a^2b^2 - 30a^2b + a^2 - 24ab^2 + 2ab - 2a + b^2)c^2 + (-30a^2b^2 + 2a^2b + 2ab^2)c + 4a^2b^2)$.

(8) $S(a,b,c) = \frac{64}{5}ac\rho_{\mathrm{xy}}(\gamma_{\mathrm{x}}+\gamma_{\mathrm{y}})((240ab^2-20ab-20b^2)c^2+(-24a^4+120a^3b-20a^2b+240ab^3-60ab^2-5ab-20b^3-5b^2+10b+24)c+2a^4-10a^3b-20ab^3-35ab^2+5ab+5b^2-2)$.

(9) $Gut(a,b,c) = \frac{64}{15}\rho_{\mathrm{xy}}^2((2880a^2b^2-480a^2b+20a^2-480ab^2+40ab+20b^2)c^3+(-288a^5+1440a^4b-480a^3b+20a^3+2880a^2b^3-1440a^2b^2+10a^2-480ab^3+260ab+268a+20b^3+10b^2-20b)c^2+(48a^5-240a^4b+40a^3b-480a^2b^3-30a^2b^2+80a^2b-5a^2+40ab^3+80ab^2-30ab-48a-5b^2)c-2a^5+10a^4b+20a^2b^3-35a^2b^2+2a)$.

(10) $Mo(a,b,c) = 96a^2c\rho_{\mathrm{xy}}(\gamma_{\mathrm{x}}+\gamma_{\mathrm{y}})((4b^2-(-1)^{(a+b)}-1)c-2b^2)$.

(11) $Mo_e(a,b,c) = \frac{32}{3}a\rho_{\mathrm{xy}}^2((144ab^2-6ab-36(-1)^{(a+b)}a-36a+3(-1)^{(a+b)}-2a^2-12b^2+5)c+3a+6ab+3(-1)^{(a+b)}a-78ab^2+6b^2)$.

(12) $w^+Mo(a,b,c) = 16a\rho_{\mathrm{xy}}(\gamma_{\mathrm{x}}+\gamma_{\mathrm{y}})(192ab^2-18ab-48(-1)^{(a+b)}a-36a+3(-1)^{(a+b)}+2a^2-12b^2+1)c^2+(6a+6(-1)^{(a+b)}a-108ab^2)c+3ab+3b^2-3(-1)^cb^2-3(-1)^cab)$.

(13) $w^+Mo_e(a,b,c) = \frac{16}{3}\rho_{\mathrm{xy}}^2(68a+24ab-336ab^2-312a^2b-420a^2-8a^3+12b^2-3(-1)^a(-1)^b+2304a^2b^2+84(-1)^a(-1)^ba-576(-1)^a(-1)^ba^2+3)c^2+(114ab^2-11a+108a^2b+108a^2+2a^3-1392a^2b^2-9(-1)^a(-1)^ba+120(-1)^a(-1)^ba^2)c+36ab^2-6ab+36a^2b-9a^2-3b^2+12a^2b^2+3(-1)^ca^2+3(-1)^cb^2-36(-1)^cab^2-36(-1)^ca^2b-6(-1)^a(-1)^ba^2+6(-1)^cab)$.

(14) $w^*Mo(a,b,c) = 8a\rho_{\mathrm{xy}}^2(\gamma_{\mathrm{x}}+\gamma_{\mathrm{y}})(24b-120a-138ab-192(-1)^{(a+b)}a+768ab^2+24(-1)^{(a+b)}+16a^2-90b^2+8)c^2+(42a+42(-1)^{(a+b)}a-468ab^2)c+21ab+21b^2-21(-1)^cb^2-21(-1)^cab)$.

(15) $w^*Mo_e(a,b,c) = \frac{8}{3}\rho_{\mathrm{xy}}^3((248a-24b+468ab-1848ab^2-2040a^2b-1350a^2+64a^3+90b^2-24(-1)^{a+b}+9216a^2b^2+480(-1)^{a+b}a-2304(-1)^{a+b}a^2+24)c^2+(516ab^2-24ab-78a+480a^2b+624a^2+12a^3-6000a^2b^2-66(-1)^{a+b}a+696(-1)^{a+b}a^2)c+252ab^2-42ab+252a^2b-63a^2-21b^2+84a^2b^2+21(-1)^ca^2+21(-1)^cb^2-252(-1)^cab^2-252(-1)^ca^2b-42(-1)^{a+b}a^2+42(-1)^cab)$.

(16) $w^+Sz_v(a,b,c) = \frac{384}{5}ac\rho_{\mathrm{xy}}(\gamma_{\mathrm{x}}+\gamma_{\mathrm{y}})^2(a^4-5a^3b-25a^3+320a^2b^3-10a^2b^2+50a^2b-20ab^3+40a-1)c^2+(5a^3-20a^2b^3-10a^2b-5a)c-40a^2b^3-5a^2b^2-5ab^3)$.

(17) $w^+Sz_e(a,b,c) = \frac{128}{15}\rho_{\mathrm{xy}}^3((-48a^5+2160a^4b-3880a^4+46080a^3b^3-16800a^3b^2+8560a^3b+585a^3-10560a^2b^3+2480a^2b^2-3465a^2b+5995a^2+800ab^3-90ab^2+110ab-907a-20b^3+10b)c^3+(16a^5-480a^4b+1355a^4-18240a^3b^3+4080a^3b^2-2810a^3b-170a^3+2720a^2b^3-300a^2b^2+880a^2b-1715a^2-100ab^3-30ab+184a)c^2+(-a^5+25a^4b-145a^4+1600a^3b^3-420a^3b^2+370a^3b+5a^3-350a^2b^3+160a^2b^2-65a^2b+160a^2+80ab^3-15ab^2-9a-5b^3)c+5a^4-500a^3b^3-10a^3b-5a^2)$.

(18) $w^+PI(a,b,c) = \frac{64}{3}\rho_{\mathrm{xy}}^2((16a^3+1152a^2b^2-216a^2b+6a^2-168ab^2+15ab-13a+6b^2)c^2+(-2a^3-504a^2b^2+45a^2b+39ab^2+2a)c+54a^2b^2)$.

(19) $w^*Sz_v(a,b,c) = \frac{192}{5}ac\rho_{\rm xy}^2(\gamma_{\rm x}+\gamma_{\rm y})^2((8a^4-40a^3b-70a^3+1280a^2b^3-70a^2b^2+140a^2b-150ab^3+160a-8)c^2+(35a^3-140a^2b^3-70a^2b-35a)c-160a^2b^3-35a^2b^2-35ab^3)$.

(20) $w^*Sz_e(a,b,c) = \frac{64}{15}\rho_{\rm xy}^4((384a^5+5760a^4b-11200a^4+184320a^3b^3-71520a^3b^2+27280a^3b+1570a^3-52320a^2b^3+14240a^2b^2-11370a^2b+23890a^2+4880ab^3-690ab^2-220ab-4184a-150b^3+80b)c^3+(40a^5-2520a^4b+6965a^4-81600a^3b^3+22800a^3b^2-14650a^3b-980a^3+15440a^2b^3-2160a^2b^2+5080a^2b-9125a^2-720ab^3-200ab+1120a)c^2+(-6a^5+170a^4b-910a^4+7840a^3b^3-4380a^3b^2+2500a^3b+35a^3-3900a^2b^3+1360a^2b^2-455a^2b+1000a^2+680ab^3-105ab^2-64a-35b^3)c+35a^4-2060a^3b^3-70a^3b-35a^2)$.

(21) $w^*PI(a,b,c) = \frac{32}{3}\rho_{\rm xy}^3((64a^3+4608a^2b^2-1116a^2b+45a^2-924ab^2+186ab-52a+45b^2-6b)c^2+(-14a^3-2232a^2b^2+246a^2b+204ab^2-6ab+14a)c+234a^2b^2)$.

Proof. We complete the proof by enumerating the Θ-classes of zeolite RHO structures and then applying Theorem 2.1. The Θ-classes of zeolite RHO structures are classified into three types as follows:

1. Front-view: $\Big\{F/_i^{ab}, F\backslash_i^{ab} : 1 \le i \le a+b-1\Big\}$, $\Big\{F|_i^{ab} : 1 \le i \le c\Big\}$ and $\big\{F-_i^{ab} : 1 \le i \le c-1\big\}$,
2. Side-view: $\{S/_i^{ac}, S\backslash_i^{ac} : 1 \le i \le a+c-1\}$, $\{S|_i^{ac} : 1 \le i \le b\}$ and $\{S-_i^{ac} : 1 \le i \le b-1\}$,
3. Top-view: $\Big\{T/_i^{bc}, T\backslash_i^{bc} : 1 \le i \le b+c-1\Big\}$, $\Big\{T|_i^{bc} : 1 \le i \le a\Big\}$ and $\big\{T-_i^{bc} : 1 \le i \le a-1\big\}$.

From the construction of forward-slash and backward-slash of Θ-classes, it is easily seen that the graph theoretical parameters of $F/_i^{ab}$ and $F\backslash_i^{ab}$ are same and similarly true for $S/_i^{ab}$, $S\backslash_i^{ab}$, $T/_i^{ab}$ and $T\backslash_i^{ab}$ of Θ-classes. In addition, the graph theoretical parameters of $S\backslash_i^{ac}$ and $T\backslash_i^{bc}$ are similar to $F\backslash_i^{ab}$ with respect to superfix variables. Also, the graph theoretical parameters of $F|_i^{ab}$, $S|_i^{ac}$ and $T|_i^{bc}$ as well as $F-_i^{ab}$, $S-_i^{ac}$ and $T-_i^{bc}$ are similar with respect to superfix variables respectively. Bearing the above relations in our mind, it is enough to perform the computation for front-view related Θ-classes and the other classes can be easily manipulated from the following equations.

If we denote $TI(a,b,c) = \sum_{i=1}^{a+b-1}\Big[TI(F/_i^{ab}) + TI(F\backslash_i^{ab})\Big] + \sum_{i=1}^{c} TI(F|_i^{ab}) + \sum_{i=1}^{c-1} TI(F-_i^{ab})$,

then $TI(a,c,b) = \sum_{i=1}^{a+c-1}\Big[TI(S/_i^{ac}) + TI(S\backslash_i^{ac})\Big] + \sum_{i=1}^{b} TI(S|_i^{ac}) + \sum_{i=1}^{b-1} TI(S-_i^{ac})$,

and $TI(b,c,a) = \sum_{i=1}^{b+c-1}\Big[TI(T/_i^{bc}) + TI(T\backslash_i^{bc})\Big] + \sum_{i=1}^{a} TI(T|_i^{bc}) + \sum_{i=1}^{a-1} TI(T-_i^{bc})$.

Combining the above three equations, we have

$$TI\big(Z(a,b,c)\big) = TI(a,b,c) + TI(a,c,b) + TI(b,c,a).$$

We now present the graph theoretical parameters related to $F/_i^{ab}$, $F\backslash_i^{ab}$, $F|_i^{ab}$ and $F-_i^{ab}$ inorder to compute the expressions of $TI(a,b,c)$. As we mentioned earlier, the expressions of $TI(a,c,b)$ and $TI(b,c,a)$ are easily derived by replacing the values of a,b and c in $TI(a,b,c)$.

The number of elements and weighted bond measures in the Θ-classes of $F/_i^{ab}$, $F\backslash_i^{ab}$, $F|_i^{ab}$ and $F-_i^{ab}$ are given below:

$$\left|F/_i^{ab}\right| = \left|F\backslash_i^{ab}\right| = \begin{cases} 8ci\rho_{\mathrm{xy}} & \text{if } 1 \le i \le a-1 \\ 8ac\rho_{\mathrm{xy}} & \text{if } a \le i \le b \\ \left|F\backslash_{a+b-i}^{ab}\right| & \text{if } b+1 \le i \le a+b-1 \end{cases}$$

$$|F|_i| = 8ab\rho_{\mathrm{xy}}, \quad 1 \le i \le c$$

$$|F-_i| = 8ab\rho_{\mathrm{xy}}, \quad 1 \le i \le c-1$$

$$w^+\left(F/_i^{ab}\right) = w^+\left(F\backslash_i^{ab}\right) = \begin{cases} (8i(8c-1)-4c)\rho_{\mathrm{xy}} & \text{if } 1 \le i \le a-1 \\ (8a(8c-1)-8c)\rho_{\mathrm{xy}} & \text{if } i = a,\ a = b \\ (8a(8c-1)-6c)\rho_{\mathrm{xy}} & \text{if } i = a,\ a < b \\ (8a(8c-1)-4c)\rho_{\mathrm{xy}} & \text{if } a < i < b \\ w^+\left(F\backslash_{a+b-i}^{ab}\right) & \text{if } b \le i \le a+b-1 \end{cases}$$

$$w^*\left(F/_i^{ab}\right) = w^*\left(F\backslash_i^{ab}\right) = \begin{cases} (4i(32c-7)-16c)\rho_{\mathrm{xy}}^2 & \text{if } 1 \le i \le a-1 \\ (4a(32c-7)-28c)\rho_{\mathrm{xy}}^2 & \text{if } i = a,\ a = b \\ (4a(32c-7)-22c)\rho_{\mathrm{xy}}^2 & \text{if } i = a,\ a < b \\ (4a(32c-7)-16c)\rho_{\mathrm{xy}}^2 & \text{if } a < i < b \\ w^*\left(F\backslash_{a+b-i}^{ab}\right) & \text{if } b \le i \le a+b-1 \end{cases}$$

$$w^+\left(F|_i\right) = 8\left(8ab-(a+b)\right)\rho_{\mathrm{xy}}, \quad 1 \le i \le c$$

$$w^*\left(F|_i\right) = 4\left(32ab-7\left(a+b\right)\right)\rho_{\mathrm{xy}}^2, \quad 1 \le i \le c$$

$$w^+\left(F-_i\right) = 64ab\rho_{\mathrm{xy}}, \quad 1 \le i \le c-1$$

$$w^*\left(F-_i\right) = 128ab\rho_{\mathrm{xy}}^2, \quad 1 \le i \le c-1$$

Finally, we present the number of vertices and edges in the components which are obtained by removal of Θ-classes from zeolites.

$$n_1\left(F/_i^{ab}\right) = n_1\left(F\backslash_i^{ab}\right) = \begin{cases} 12ci^2(\gamma_{\mathrm{x}}+\gamma_{\mathrm{y}}) & \text{if } 1 \le i \le a-1 \\ 12ac(2i-a)(\gamma_{\mathrm{x}}+\gamma_{\mathrm{y}}) & \text{if } a \le i \le b \\ n_1\left(F\backslash_{a+b-i}^{ab}\right) & \text{if } b+1 \le i \le a+b-1 \end{cases}$$

$$n_2\left(F/_i^{ab}\right) = n_2\left(F\backslash_i^{ab}\right) = |V_\gamma(RHO(a,b,c))| - n_1\left(F\backslash_i^{ab}\right)$$

$$m_1\left(F/_i^{ab}\right) = m_1\left(F\backslash_i^{ab}\right) = \begin{cases} 4((12c-1)i^2-3ci)\rho_{\mathrm{xy}} & \text{if } 1 \le i \le a-1 \\ 4(2(12ac-a-c)i-ac(12a+1)+a^2)\rho_{\mathrm{xy}} & \text{if } a \le i \le b \\ m_1\left(F\backslash_{a+b-i}^{ab}\right) & \text{if } b+1 \le i \le a+b-1 \end{cases}$$

$$m_2\left(F/_i^{ab}\right) = m_2\left(F\backslash_i^{ab}\right) = |E_\rho(RHO(a,b,c))| - m_1\left(F\backslash_i^{ab}\right) - \left|F\backslash_i^{ab}\right|$$

For $1 \le i \le c$,

$$\begin{aligned} n_1\left(F|_i\right) &= 12ab(2i-1)(\gamma_{\mathrm{x}}+\gamma_{\mathrm{y}}), \\ n_2\left(F|_i\right) &= |V_\gamma(RHO(a,b,c))| - n_1\left(F|_i\right), \\ m_1\left(F|_i\right) &= 4(2(12ab-a-b)i-(14ab-a-b))\rho_{\mathrm{xy}}, \\ m_2\left(F|_i\right) &= |E_\rho(RHO(a,b,c))| - m_1\left(F|_i\right) - |F|_i|. \end{aligned}$$

For $1 \le i \le c-1$,

$$\begin{aligned} n_1\left(F{-_i}\right) &= 24abi(\gamma_{\mathrm{x}}+\gamma_{\mathrm{y}}), \\ n_2\left(F{-_i}\right) &= |V_\gamma(RHO(a,b,c))| - n_1\left(F{-_i}\right), \\ m_1\left(F{-_i}\right) &= 8((12ab-(a+b))i-ab)\rho_{\mathrm{xy}}, \\ m_2\left(F{-_i}\right) &= |E_\rho(RHO(a,b,c))| - m_1\left(F{-_i}\right) - |F{-_i}|. \end{aligned}$$

Then, $TI(a,b,c) = 4\sum_{i=1}^{a-1} TI(F/_i^{ab}) + 2\sum_{i=a}^{b} TI(F\backslash_i^{ab}) + \sum_{i=1}^{c} TI(FB|_i^{ab}) + \sum_{i=1}^{c-1} TI(F-_i^{ab})$, which completes the proof. □

4.1 Degree-based Topological Indices

In this section, we use the edge partition technique based on the degrees of terminal vertices of each edge to find the expressions of degree-based topological indices of the zeolite RHO materials. Since zeolite RHO contains only ρ_{xy} bond type, it is sufficient to consider the computation of degree-based

indices without weights. We now partition the edge set of zeolite $RHO(a,b,c)$ as follows:

Let $E_1 = \{uv \in E\big(RHO(a,b,c)\big) : \big(\deg_G(u), \deg_G(v)\big) = (3,3)\}$,

$E_2 = \{uv \in E\big(RHO(a,b,c)\big) : \big(\deg_G(u), \deg_G(v)\big) = (3,4)\}$,

$E_3 = \{uv \in E\big(RHO(a,b,c)\big) : \big(\deg_G(u), \deg_G(v)\big) = (4,4)\}$.

Then $E\big(RHO(a,b,c)\big) = E_1 \cup E_2 \cup E_3$ and

$\big|E_1\big| = 8(2(ab+bc+ac)+(a+b+c))$,

$\big|E_2\big| = 16((ab+bc+ac)-(a+b+c))$,

$\big|E_3\big| = 8(12abc-5(ab+bc+ac)+(a+b+c))$.

In addition, there are $16(ab+ac+bc)$ vertices of degree 3 and $48abc-16(ab+ac+bc)$ vertices are of degree 4. We now present the degree-based topological measures of zeolite RHO materials in view of the above edge partition by simple mathematical calculations.

Theorem 4.3. *Let G be a Zeolite RHO materials $RHO(a,b,c)$ where $a,b,c \geq 1$. Then,*

(1) $M_1(G) = 16(48abc-7(ab+bc+ca))$.

(2) $M_2(G) = 8(192abc-38(ab+bc+ca)+(a+b+c))$.

(3) $R(G) = \frac{2}{3}(36abc+(4\sqrt{3}-7)(ab+bc+ca)-(4\sqrt{3}-7)(a+b+c))$.

(4) $ABC(G) = \frac{2}{3}(36\sqrt{6}abc+(4\sqrt{15}-15\sqrt{6}+16)(ab+bc+ca)+(3\sqrt{6}-4\sqrt{15}+8)(a+b+c))$.

(5) $H(G) = \frac{2}{21}(252abc-(ab+bc+ca)+(a+b+c))$.

(6) $HM(G) = \frac{2}{21}(252\sqrt{2}abc+(28\sqrt{6}-105\sqrt{2}+24\sqrt{7})(ab+bc+ca)+(21\sqrt{2}+14\sqrt{6}-24\sqrt{7})(a+b+c))$.

(7) $SC(G) = 16(384abc-75(ab+bc+ca)+(a+b+c))$.

(8) $GA(G) = \frac{8}{7}(84abc+(8\sqrt{3}-21)(ab+bc+ca)-(8\sqrt{3}-14)(a+b+c))$.

(9) $irr(G) = 16((ab+bc+ca)-(a+b+c))$.

(10) $\sigma(G) = 16((ab+bc+ca)-(a+b+c))$.

(11) $F(G) = 16(192abc-37(ab+bc+ca))$.

(12) $SDD(G) = \frac{4}{3}(144abc-11(ab+bc+ca)-(a+b+c))$.

4.2 Numerical Values

By considering the relativistic parameters as $\gamma_x = \gamma_y = \rho_{xy} = 1$, the numerical topological descriptor values are presented in Tables 2 and 3 and the comparative study between the descriptors are displayed in Figures 5 and 6. The numerical results for the topological indices derived from the expressions were also validated against the results computed from the TopoChemie-2020 software [67].

Table 2: TI values of $RHO(a, b)$

TI	$a = 1$		$a = 2$		$a = 3$	
	$b = 2$	$b = 3$	$b = 3$	$b = 4$	$b = 4$	$b = 5$
W	28800	84672	402048	854784	2195712	3918528
W_e	59520	189312	1007968	2228064	5985760	10923520
W_{ev}	41472	126720	637440	1381248	3628032	6546048
Sz_v	304128	1009152	7805952	18413568	61728768	120319488
Sz_e	624128	2206720	19445248	47286272	166816256	331005952
Sz_{ev}	436224	1492992	12334080	29531136	101529600	199640064
PI	21376	50432	227712	413440	967296	1529856
S	180480	540288	2690304	5776896	15088128	27088512
Gut	282560	861504	4497728	9756032	25910336	46801472
M	3840	8448	56064	102912	238080	369408
Mo_e	6400	14080	98560	181504	423936	659200
w^+Mo	24192	54528	386304	716544	1687680	2635776
w^+Mo_e	40320	90880	679232	1264000	3005568	4704128
w^*Mo	38016	88320	670464	1258752	3019392	4748544
w^*Mo_e	63360	147200	1179072	2220864	5377920	8475904
w^+Sz_v	1990656	6750720	55480320	132000768	450708480	882556416
w^+Sz_e	4090368	14780416	138350592	339198720	1218791936	2428919296
w^+PI	139520	335616	1604736	2938496	6993280	11114496
w^*Sz_v	3253248	11326464	99753984	239459328	833292288	1639111680
w^*Sz_e	6695424	24842752	249042176	615808896	2255059200	4513345536
w^*PI	227328	560000	2857728	5280384	12790912	20429568

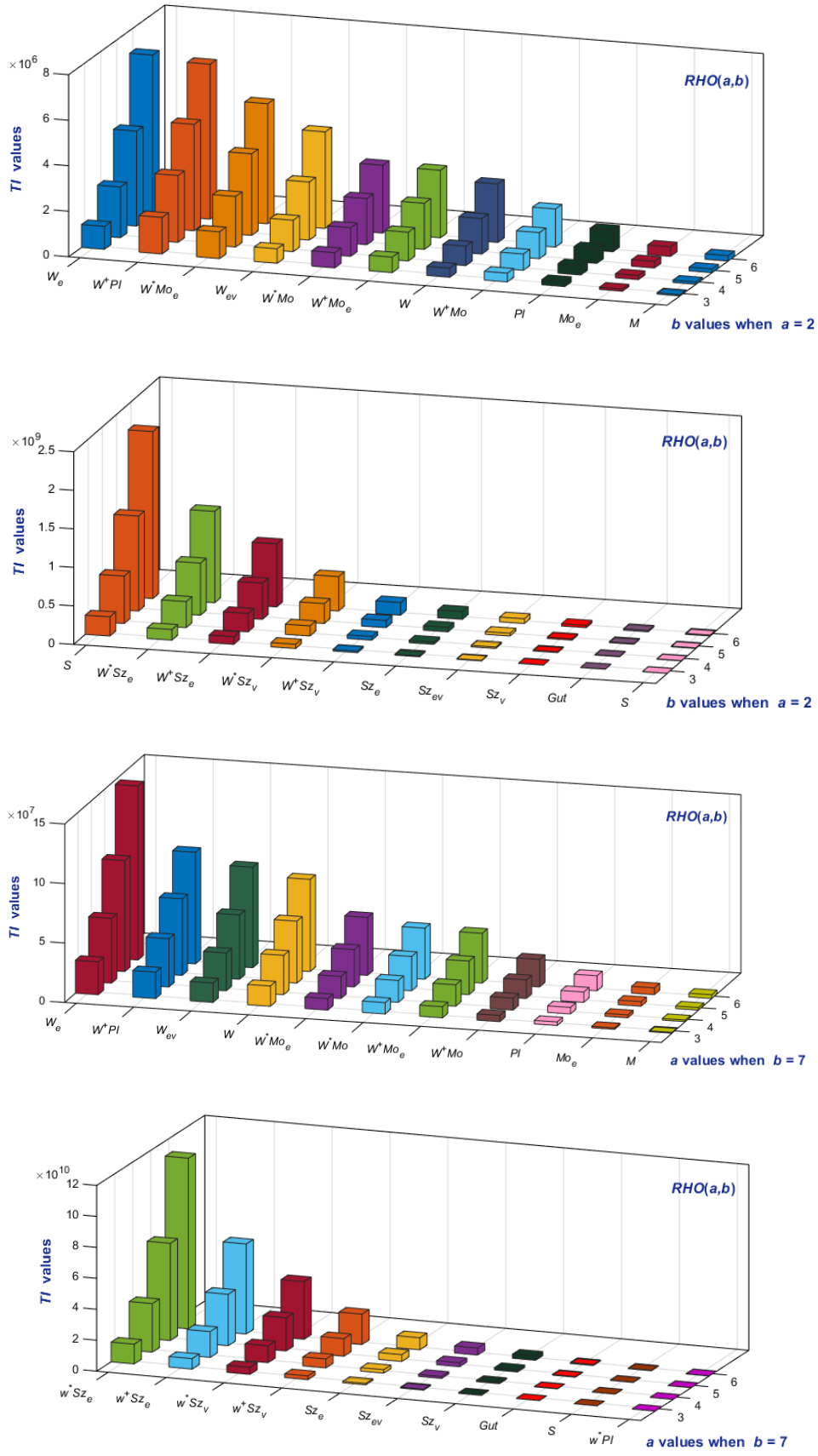

Figure 5: Comparison of TI values for $RHO(a, b)$

Table 3: TI values of $RHO(a, b, c)$ when $a = b = c$

$\boldsymbol{TI}$	$\boldsymbol{a = 2}$	$\boldsymbol{a = 3}$	$\boldsymbol{a = 4}$	$\boldsymbol{a = 5}$	$\boldsymbol{a = 6}$
M_1	4800	17712	43776	87600	153792
M_2	8688	33336	83808	169320	299088
R	191.71	647.14	1534.28	2997.13	5179.69
ABC	427.72	1491.90	3593.26	7084.51	12318.40
H	191.43	646.29	1532.57	2994.29	5175.43
SC	253	875	2098	4126	7163
HM	34848	133632	335808	678240	1197792
GA	671.01	2373.05	5754.09	11381.25	19857.23
irr	96	288	576	960	1440
σ	96	288	576	960	1440
F	17472	66960	168192	339600	599616
SDD	1352	4776	11568	22880	39864
W	230400	3986496	30007296	143409600	514501632
W_e	609984	12151936	98041728	488254464	1800082496
W_{ev}	375552	6966144	54266880	264698880	962581248
Sz_v	6340608	242237952	3222798336	24004800000	123846672384
Sz_e	16960512	743851008	10586972160	82073395200	434794595328
Sz_{ev}	10383360	424756224	5843386368	44397312000	232091578368
PI	144384	1833984	10854400	42688000	130046976
S	1588224	28891008	222965760	1081595520	3919002624
Gut	2734848	52323520	414080512	2039025856	7462009088
M	30720	435456	2654208	10560000	32348160
Mo_e	55808	817920	5066752	20352000	62737920
w^+Mo	215040	3227904	20054016	80832000	249440256
w^+Mo_e	390656	6063744	38285312	155795200	483801600
w^*Mo	379392	6027264	38129664	155520000	483134976
w^*Mo_e	689280	11324160	72800768	299769600	937111680
w^+Sz_v	45563904	1815478272	24600379392	185125248000	961403240448
w^+Sz_e	122000384	5576954880	80826331136	633005153280	3375410525184
w^+PI	1031168	13670016	82487296	328006400	1006411776

TI	$a=2$	$a=3$	$a=4$	$a=5$	$a=6$
w^*Sz_v	83128320	3438236160	47324528640	359220672000	1875784200192
w^*Sz_e	222835456	10565968896	155513768960	1228396989440	6586032925440
w^*PI	1865984	25724928	157905920	633958400	1957142784

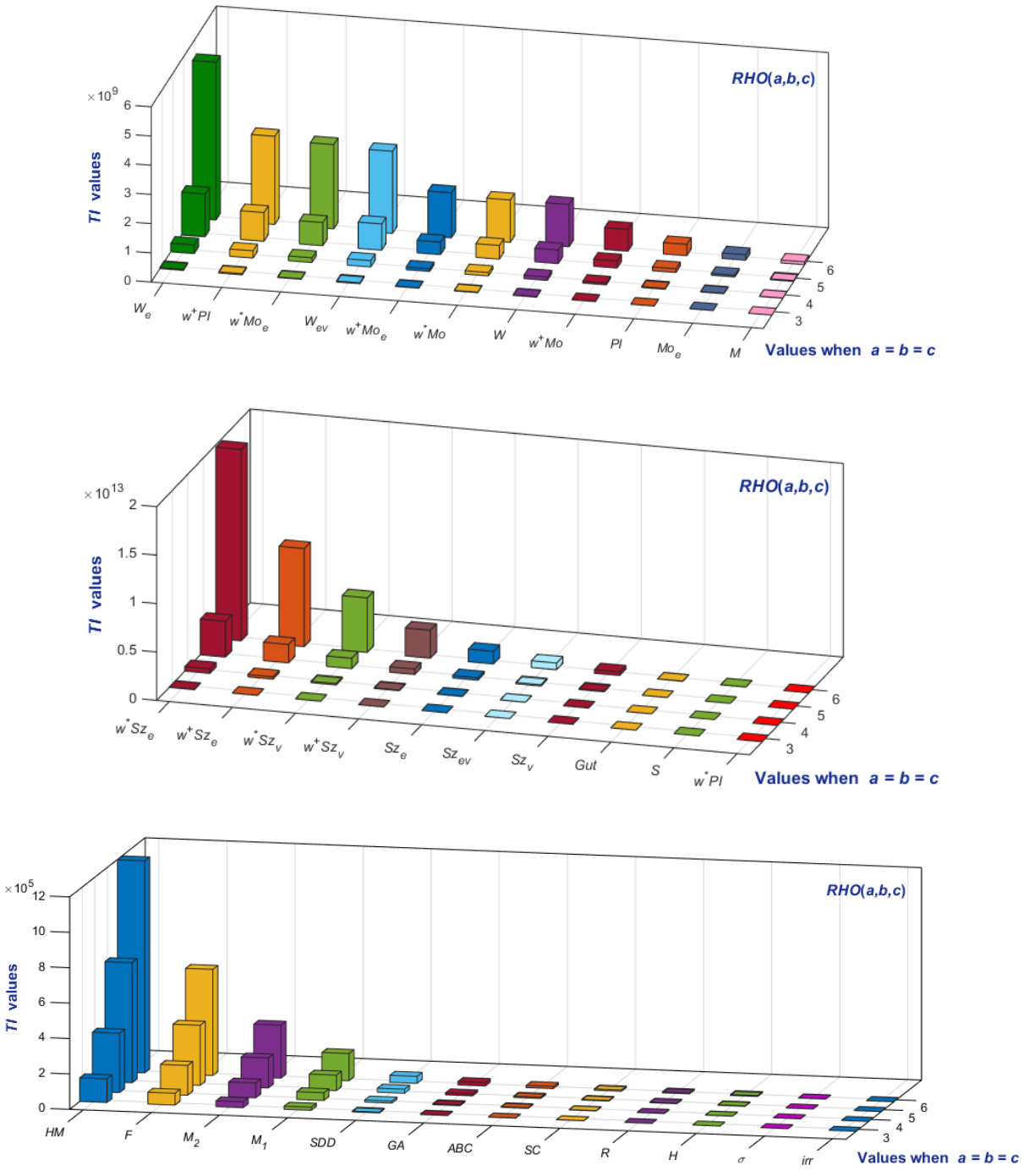

Figure 6: Comparison of TI values for $RHO(a,b,c)$

One can visualize from the above numerical values and 3D-bar graphs that the degree-based TIs have the smaller quantity values compared to distance-based indices. Among all the distance-based TIs, Mostar type indices acquire the least values while Szeged type indices expose the largest values implying the peripheral perfection of the materials. On the other hand, the correlation between the pairs of TIs such as (M_1, M_2), (R, ABC), (W, W_e), (S, Gut), (M, Mo_e) and etc., was found to be greater than 0.99. Hence, all the acquired topological descriptors are highly significant for the characterization of the QSAR properties of zeolite frameworks. Relativistic effects in both scalar form and vector form (spin-orbit coupling) are extremely important for molecules and materials that contain very heavy atoms [24, 25]. Both computational and experimental studies have been carried out on such molecules with heavy atoms [17, 18, 24–27, 67–70], and all of these studies have demonstrated the importance of relativistic effects including spin-orbit coupling. Consequently, the techniques developed in the current study can provide rapid quantitative measures of phase transformations and other structural and topological modifications that occur in materials through the incorporation of such heavy atoms through sorption, environmental pollutants and so forth. Such relativistic computations of the topological indices of these materials would involve two-component Wannier function spinors obtained from localization of Bloch spinors by localization techniques such as the Pipek-Mezey localization technique [71]. The technique would yield a number of localized properties including localized charges, populations and bond parameters which can then be used in the relativistic topological indices formulated in this study.

5 Conclusion

In this study we have computed relativistic structural descriptors for 3D zeolite RHO frameworks by employing cut methods for vertex and edge weighted molecular graphs. These materials exhibit extremely complex framework of topologies in multiple layers, cages and pores. Such relativistic topological descriptors of zeolite RHOs can provide for QSAR correlations for rapid computations of their physico chemical properties and thus enhance future applications of these materials for catalysis and sorptions. These techniques can also pave the way for future synthesis of novel and complex 2D and 3D structures comprising of tunnels and cages. An important feature of the developments considered here is that relativistic effects are included in here. Thus applications to a number of structural and reactivity problems pertaining to very heavy elements are feasible. For example, environmental remediation of mercury ions and actinyl ions found in environmental and high-level nuclear wastes requires such developments and consequently, the developed techniques are of paramount importance to the environmental management of pollutants, green-house gases and mitigation of heavy metal

toxins including the ones in high level nuclear wastes. Moreover the developed topological indices that have the capability to include relativistic effects would be especially useful in the characterization of morphological changes to the materials that occur by the incorporation of heavier elements into the zeolite. The topological techniques can also provide quantitative measures for phase transitions and other modifications to the materials through interaction with chemicals, pollutants, and heavy metal ions.

References

[1] J.B. Parise, E. Prince, The structure of cesium-exchanged zeolite-Rho at 293K and 493K determined from high resolution neutron powder data, Mater. Res. Bull. **18** (1983) 841–852.

[2] D.R. Corbin, L. Abrams, C.A. Jones, M.M. Eddy, W.T.A. Harrison, G.D. Stucky, D.E. Cox, Flexibility of the zeolite Rho framework, in situ X-ray and neutron powder structural characterization of divalent cation-exchanged zeolite Rho, J. Am. Chem. Soc. **112** (1990) 4821–4830.

[3] G.M. Johnson, B.A. Reisner, A. Tripathi, D.R. Corbin, B.H. Toby, J.B. Parise, Flexibility and cation distribution upon lithium exchange of aluminosilicate and alumino germanate materials with the Rho topology, Chem. Mater. **11** (1999) 2780–2787.

[4] G.M. Johnson, A. Tripathi, J.B. Parise, Synthesis and structure of a microporous alumino germanate with the zeolite Rho topology, Micropor. Mesopor. Mat. **28** (1999) 139–154.

[5] H. Sun, M. Wu, F. Han, W.H. Wang, W. Wang, X. Luo , H. Chen, Crystallization of high silica RHO Zeolite with self-assembled Cs^{+}-18-crown-6 sandwich complex, Cryst. Growth Des. **19**(6) (2019) 3389–3396.

[6] L. Abrams, D.R. Corbin, M. Keane Jr., Synthesis of dimethylamine by zeolite Rho: A rational basis for selectivity, J. Catal. **126** (1990) 610–618.

[7] D.R. Corbin, S. Schwarz, G. C. Sonnichsen, Methylamine ssynthesis: A review, Catal. Today **37** (1997) 71–102.

[8] L.H. Callanan, C.T. O'Connor, E. Van Steen, The effect of the adsorption properties of steamed zeolite Rho on its methanol amination activity, Micropor. Mesopor. Mat. **35–36** (2000) 163–172.

[9] L.H. Callanan, E. Van Steen, C.T. O'Connor, Improved selectivity to lower substituted methylamines using hydrothermally treated zeolite Rho, Catal. Today **49** (1999) 229–235.

[10] H.Y. Jeon, C.H. Shin, H.J. Jung, S.B. Hong, Catalytic evaluation of small-pore molecular sieves with different framework topologies for the synthesis of methylamines, Appl. Catal. A-Gen. **305** (2006) 70–78.

[11] S. Altwasser, R. Glaser, J. Weitkamp, Ruthenium-containing small- pore zeolites for shape-selective catalysis, Micropor. Mesopor. Mat. **104** (2007) 281–288.

[12] V.V. Krishnana, S.L. Suib, D.R. Corbin, S. Schwarz, G.E.Jones, Encapsulation studies of hydrogenon cadmium exchanged zeolite Rho at atmospheric pressure, Catal. Today **31** (1996) 199–205.

[13] H.W. Langmi, A. Walton, M.M. Al-Mamouri, S.R. Johnson, D. Book, J.D. Speight, P.P. Edwards, I. Gameson, P.A. Anderson, I.R. Harris, Hydrogen adsorption in zeolites A, X, Y and Rho, J. Alloys Compd. **356–357** (2003) 710–715.

[14] H.W. Langmi, D. Book, A. Walton, S.R. Johnson, M.M. Al-Mamouri, J.D. Speight, P.P. Edwards, I.R. Harris, P.A. Anderson, Hydrogen storage in ion-exchanged zeolites, J. Alloys Compd. **404–406** (2005) 637–642.

[15] S. Araki, Y. Kiyohara, S. Tanaka, Y. Miyake, Adsorption of carbon dioxide and nitrogen on zeolite rho prepared by hydrothermal synthesis using 18-crown-6 ether, J. Colloid Interface Sci. **376** (2012) 28–33.

[16] T.Y.S. Ng, T.L. Chew, Y.F. Yeong, Z.A. Jawad, C.D. Ho, Zeolite RHO synthesis accelerated by ultrasonic irradiation treatment, Sci. Rep. **9**(1) (2019) 1–11.

[17] L.K. Schwaiger, T. Parsons-Moss, A. Hubaud, H. Tueysuez, K. Balasubramanian, P. Yang, H. Nitsche, Actinide and lanthanide complexation by organically modified mesoporous silica (In Abstracts of papers), Amer. Chemical Soc. **239** (2010) 1155.

[18] T. Parsons-Moss, L. K. Schwaiger, A. Hubaud, Y. J. Hu, H. Tuysuz, P. Yang, K. Balasubramanian, H. Nitsche, Plutonium complexation by phosphonate-functionalized mesoporous silica, 2010 (No. LLNL-CONF–461496) United States.

[19] Y. Pan, P. Dong, Bromine in scapolite-group minerals and sodalite: XRF microprobe analysis, exchange experiments, and application to skarn deposits, Canad. Mineral. **41** (2003) 529–540.

[20] M. O'Keeffe, N-Dimensional Diamond, Sodalite and Rare Sphere Packings, Acta Cryst. **(**47) (1991) 748–753.

[21] R. Xu, W. Pang, J. Yu , Q. Huo, J. Chen, Chemistry of Zeolites and Related Porous Materials: Synthesis and Structure, Clementi loop Singapore, John Wiley & Sons, 2007.

[22] C. Jiri, V.B. Herman, C. Avelino, S. Ferdi, Introduction to zeolite science and practice, Stud. Surf. Sci. **2**(1) (2007) 1058–1065.

[23] M. Arockiaraj, J. Clement, D. Paul, K. Balasubramanian, Quantitative structural descriptors of sodalite materials, J. Mol. Struct. **1223** (2021) e128766.

[24] K. Balasubramanian, Relativistic Effects in Chemistry, Part A: Theory & Techniques, Wiley-Interscience, New York, 1997.

[25] K. Balasubramanian, Relativistic Effects in Chemistry, Parts B: Applications, Wiley-Interscience: New York, 1997.

[26] D. Majumdar, K. Balasubramanian, H. Nitsche, A comparative theoretical study of bonding in UO_2^{2+}, $UO_2{}^+$, UO_2, $UO_2{}^-$, OUCO, $O_2U(CO)_2$ and UO_2CO_3. Chem. Phys. Lett. **361** (2002) 143–151.

[27] K. Balasubramanian, CASSCF/CI calculations of electronic states and potential energy surfaces of PtH_2, J. Chem. Phys. **87**(5) (1987) 2800–2805.

[28] H. Wiener, Structural determination of paraffin boiling points, J. Am. Chem. Soc. **69**(1) (1947)17–20.

[29] M. Randić, On characterization of molecular branching, J. Amer. Chem. Soc. **97**(23) (1975) 6609–6615.

[30] M.H. Khalifeh, H. Yousefi-Azari, A.R. Ashrafi, S.G. Wagner, Some new results on distance-based graph invariants, European J. Combin. **30**(5) (2009) 1149–1163.

[31] H.P. Schultz, Topological organic chemistry. 1. Graph theory and topological indices of alkanes, J. Chem. Inf. Comput. Sci. **29**(3) (1989) 227–228.

[32] I. Gutman, Selected properties of the Schultz molecular topological index, J. Chem. Inf. Comput. Sci. **(**34) (1994) 1087–1089.

[33] I. Gutman, A formula for the Wiener number of trees and its extension to graphs containing cycles, Graph Theory Notes N. Y. **27**(1) (1994) 9–15.

[34] I. Gutman, A.R. Ashrafi, The edge version of the Szeged index, Croat. Chem. Acta **81**(2) (2008) 263–266.

[35] P.V. Khadikar, S. Karmarkar, V.K. Agrawal, A novel PI index and its applications to QSPR/QSAR studies, J. Chem. Inf. Comput. Sci. **41**(4) (2001) 934–949.

[36] M.H. Khalifeh, H. Yousefi-Azari, A.R. Ashrafi, I. Gutman, The edge Szeged index of product graphs, Croat. Chem. Acta **81**(2) (2008) 277–281.

[37] I. Gutman, N.Trinajstić, Graph theory and molecular orbitals. Total π-electron energy of alternant hydrocarbons Chem. Phys. Lett. **17**(4) (1972) 535–538.

[38] E. Estrada, L. Torres, L. Rodríguez, I. Gutman, An atom-bond connectivity index: Modelling the enthalpy of formation of alkanes Indian J. Chem. **37A**(10) (1998) 849–855.

[39] S. Fajtlowicz, On conjectures of Graffiti-II Congr. Numer. **60** (1987) 187–197.

[40] B. Zhou, N. Trinajstić, On a novel connectivity index J. Math. Chem. **46**(4) (2009) 1252–1270.

[41] D. Vukičević, B. Furtula, Topological index based on the ratios of geometrical and arithmetical means of end-vertex degrees of edges, J. Math. Chem. **46**(4) (2009) 1369–1376.

[42] M.O. Albertson, The irregularity of a graph, Ars Comb. **46** (1997) 219–225.

[43] I. Gutman, M. Togan, A. Yurttas, A. S. Cevik, I.N. Cangul, Inverse problem for sigma index, MATCH Commun. Math. Comput. Chem. **79** (2018) 491–508.

[44] B. Furtula, I. Gutman, A forgotten topological index, J. Math. Chem. **53** (2015) 1184–1190.

[45] A. Vasilyev, Upper and lower bounds of symmetric division deg index, Iranian J. Math. Chem. **5**(2) (2014) 91–98.

[46] G.H. Shirdel, H. Rezapour, A.M. Sayadi, The hyper-Zagreb index of graph operations, Iranian J. Math. Chem. **4**(2) (2013) 213-220.

[47] N. Tratnik, Computing weighted Szeged and PI indices from quotient graphs, Int. J. Quantum Chem. **119**(21) (2019) e26006.

[48] M. Arockiaraj, J. Clement, N. Tratnik, Mostar indices of carbon nanostructures and circumscribed donut benzenoid systems, Int. J. Quantum Chem. **119**(24) (2019) e26043.

[49] T. Došlić, I. Martinjak, R. Škrekovski, S. Tipurić Spužević, I. Zubac, Mostar index, J. Math. Chem. **56** (2018) 2995–3013.

[50] M. Arockiaraj, J. Clement, N. Tratnik, S. Mushtaq, K. Balasubramanian, Weighted Mostar indices as measures of molecular peripheral shapes with applications to graphene, graphyne and graphdiyne nanoribbons, SAR QSAR Environ. Res. **31**(3) (2020) 187–208.

[51] M. Arockiaraj, J. Clement, D. Paul, K. Balasubramanian, Relativistic distance based topological descriptors of Linde type A zeolites and their doped structures with very heavy elements, Mol. Phys. **119**(3) (2021) e1798529.

[52] S. Klavžar, I. Gutman, B. Mohar, Labeling of benzenoid systems which reflects the vertex-distance relation, J. Chem. Inf. Comput. Sci. **35**(3) (1995) 590–593.

[53] S. Klavžar, M. J. Nadjafi-Arani, Cut method: update on recent developments and equivalence of independent approaches, Curr. Org. Chem. **19** (2015) 348–358.

[54] D. Djoković, Distance preserving subgraphs of hypercubes, J. Combin. Theory Ser. B **14**(3) (1973) 263–267.

[55] P. Winkler, Isometric embeddings in products of complete graphs, Discrete Appl. Math. **7**(2) (1984) 221–225.

[56] S. Klavžar, M.J. Nadjafi-Arani, Wiener index in weighted graphs via unification of Θ^*-classes European J. Combin. **36** (2014) 71–76.

[57] N. Tratnik, Computing the Mostar index in networks with applications to molecular graphs, (2019) arXiv:1904.04131.

[58] M. Arockiaraj, J. Clement, K. Balasubramanian, Analytical expressions for topological properties of polycyclic benzenoid networks, J. Chemom. **30**(11) (2016) 682-697.

[59] P.E. John, P.V. Khadikar, J. Singh, A method of computing the PI index of benzenoid hydrocarbons using orthogonal cuts, J. Math. Chem. **42**(1) (2007) 37–45.

[60] M.H. Khalifeh, H. Yousefi-Azari, A.R. Ashrafi, Another aspect of graph invariants depending on the path metric and an application in nanoscience, Comput. Math. Appl. **60**(8) (2010) 2460–2468.

[61] S. Klavžar, I. Gutman, B. Mohar, Labelling of benzenoid systems which reflects the vertex-distance relation, J. Chem. Inf. Comput. Sci. **35**(3) (1995) 590–593.

[62] P. Manuel, I. Rajasingh, M. Arockiaraj, Total-Szeged index of C_4-nanotubes, C_4-nanotori and denrimer nanostars, J. Comput. Theor. Nanosci. **10**(2) (2013) 405–411.

[63] H. Yousefi-Azari, M.H. Khalifeh, A.R. Ashrafi, Calculating the edge Wiener and Szeged indices of graphs, J. Comput. Appl. Math. **235**(16) (2011) 4866–4870.

[64] I. Gutman, S. Klavžar, An algorithm for the calculation of Szeged index of benzenoid hydrocarbons, J. Chem. Inf. Comput. Sci. **35**(6) (1995) 1011–1014.

[65] R. Hammack, W. Imrich, S. Klavžar, Handbook of Product Graphs, Second Edition, CRC Press, Boca Raton, FL, 2011.

[66] S. Klavžar, S. Shpectorov, Tribes of cubic partial cubes, Discrete Math. Theor. Comput. Sci. **9** (2007) 273–291.

[67] K.Balasubramanian, TopoChemie-2020, Package for the computation of Topological Indices, Graph Polynomials, Spectra and Automorphism Partitions, 2020.

[68] X. Li, W. Zheng, A. Buonaugurio, A. Buytendyk, K. Bowen, K. Balasubramanian, Photoelectron spectroscopy of the molecular anions, ZrO^-, HfO^-, $HfHO^-$, and HfO_2H^-, J. Chem. Phys. **136** (2012) 154306.

[69] M. Benavides-Garcia, K. Balasubramanian. Spectroscopic constants and potential energy curves for OsH. J. Mol. Spectrosc. **150**(1) (1991) 271–279.

[70] R. Guo, K. Balasubramanian, X. Wang, L. Andrews, Infrared vibronic absorption spectrum and spin–orbit calculations of the upper spin–orbit component of the Au_3 ground state, J. Chem. Phys. **117** (2002) 1614.

[71] J. Pipek, P.G. Mezey, A fast intrinsic localization procedure applicable for ab initio and semiempirical linear combination of atomic orbital wave functions, J. Chem. Phys. **90** (1989) 4916.